UNIVERSITY OF OKLAHOMA

GRADUATE COLLEGE

INTEGRATED DIAGENETIC AND PALEOMAGNETIC STUDY OF THE SYCAMORE FORMATION IN THE SOUTHERN FLANK OF THE ARBUCKLE ANTICLINE, SOUTHERN OKLAHOMA

A THESIS

SUBMITTED TO THE GRADUATE FACULTY

in partial fulfillment of the requirements for the

Degree of

MASTER OF SCIENCE

By

DELCIO SALOMÃO DOMBASSI TEIXEIRA

Norman, Oklahoma

2021

INTEGRATED DIAGENETIC AND PALEOMAGNETIC STUDY OF THE SYCAMORE FORMATION IN THE SOUTHERN FLANK OF THE ARBUCKLE ANTICLINE, SOUTHERN OKLAHOMA

A THESIS APPROVED FOR THE

SCHOOL OF GEOSCIENCES

BY THE COMMITTEE CONSISTING OF

Dr. R. Douglas Elmore, Chair

Dr. Shannon Dulin

Dr. Xiaolei Liu

To my mom for being the biggest inspiration anyone could have – I often pray that you are able to know some of my joys, and I hope this makes you proud…

To my beloved grandparents, Maria Amélia and Alexandre Dombassi, thank you for being the gift to my life and the best educators. You have been an incredible source of wisdom, support, and endless love!

ACKNOWLEDGMENTS

First and foremost, all praise goes to God for blessing me with an opportunity to continue my studies abroad and for being my strength and shield during this journey.

I would like to express my sincere gratitude to Dr. Roger Slatt who has believed in me with no hesitation since the beginning of my college career. Thank you Dr. Slatt for the opportunity to conduct an undergraduate research project under your guidance and for encouraging me to attend a graduate program. Dr. Slatt's passion for geology has inspired me to join his research group, Institute of Reservoir Characterization (IRC), during my first year as a graduate student, and I am very thankful for all the support and learning experience. You are dearly missed, Dr. Slatt!

My profound gratitude and appreciation is extended to my advisor, Dr. Elmore, for the opportunity to join his research group at a delicate time and for playing an instrumental role during the transition period. Dr. Elmore's constant guidance and invaluable mentoring were crucial to the completion of this thesis project. I would not be able to complete a thesis project especially during a pandemic if it was not for Dr. Elmore's support and continuous words of encouragement. I really appreciate your support, patience, and all the contributions in the course of this project.

I wish to thank my thesis committee members, Dr. Shannon Dulin and Dr. Xiaolei Liu, for their valuable comments during the review and discussion of my thesis. Moreover, I would like to express my deepest appreciation to Brian Cardott for providing me with valuable literature references from my study area.

My heartfelt appreciation also goes to my peers in the research group- Matt, Katie, Marta, Emily, and Liz. Thank you to each one of you for your valuable contributions, field assistance, and emotional support. A special thanks to Matt, Katie, and Marta for always being available to help and provide constructive criticism. I would like to extend my utmost gratitude to the former

members of the IRC, especially to Benmadi Milad for allowing me to use some of his Sycamore thin sections, and David Duarte for the incessant support and constant effort to always answer my questions.

A multitude of gratitude to the Mewbourne College of Earth and Energy; particularly, thank you to Dean Stice, Dr. Gerilyn Soreghan, and all the donors for their support and good heartedness that has made this journey possible. I am also grateful for the faculty and staff at the School of Geosciences. Furthermore, my deepest gratitude to Mr. James Gibbs, Mrs. Judy Gibbs, DeGolyer & MacNaughton, and the Geological Society of America for their generosity in providing me with scholarship and research grants. I also would like to thank the supportive international community at OU including the International Advisory Committee and the College of International Studies.

I feel grateful to have incredible friends and colleagues whose friendship has made this journey an unforgettable experience: Dalila, Nawik, Aires, Tara, Eduardo, Alisan, Denise, Joseth, Fábio, Andreia, Olivia, Guliziran, Karelia, Hannah, Cody, Grace, Brittany, Sarah, Roberto, Nishit, Hussain, Anna, Daana, Yara, Ducha, Leticia, and Aditya. Thank you to each one of you for the positive influence you have had in my life and for your endless support and motivation. I am deeply appreciative of the members of the Zoom focus group; specifically, Chelsey and Cansu for keeping me inspired and motivated throughout this journey. My warmest thanks to the brethren for keeping me in their prayers and for their kind acts of support.

I am forever indebted to my family for being the best support system! Thank you to my parents, my grandmother, Papa Gamboa, my aunts Inês and Beth, and my sisters for showing me that with hard work and dedication, we can achieve our dreams. Thank you very much!

TABLE OF CONTENTS

LIST OF FIGURES

LIST OF TABLES

ABSTRACT

This study aimed to evaluate the paragenesis of the Mississippian Sycamore Formation in the southern Flank of the Arbuckle Anticline in order to document the extent of diagenetic alteration in outcrop, assess the factors controlling the diagenesis (open vs. closed), and determine the timing of diagenetic events. Core plugs were collected from multiple sites in the southern flank of the Arbuckle Anticline (I-35 outcrop) for thin sections as well as for anisotropy of magnetic susceptibility (AMS) and paleomagnetic analysis. Thin section and scanning electron microscope (SEM) analysis were used to identify the microfacies, diagenetic features, pore types, fracture mineralization, and the parageneses based on cross cutting and textural relationships. The AMS analysis was performed to obtain information about the fabric of the rock and level of alteration. Paleomagnetic analysis was used to identify the magnetic components and date any chemical remanent magnetizations (CRMs). The results of this study contribute to the understanding of micro-textural fabric alteration and add insights into the complexities related to pore evolution of the Mississippian strata.

The Sycamore Formation is characterized by five microfacies- argillaceous mudrock, siliceous mudrock, calcareous mudrock, calcitic siltstone, and calcite cemented siltstone. Major diagenetic events include calcite cement precipitation, feldspar dissolution, clay alteration, styliolitization, and fracturing. Early calcite cement occludes most of the porosity in calcite cemented siltstones, and feldspar dissolution is more predominant in calcitic siltstones. Inverse AMS fabrics are concordant with precipitation of ferroan dolomite as a result of alteration by iron-rich dolomitizing fluids. A secondary magnetization, interpreted to reside in magnetite, is present in the Sycamore Formation and the upper Woodford Shale, but determining the timing of remagnetization was not possible because a fold test could not be performed. The Sycamore Formation is interpreted to have been a closed diagenetic system with internal fluids derived from

the mudrock facies. During burial, the Sycamore Formation might have evolved into an open system with the introduction of external iron-rich dolomitizing fluids and acidic fluids from organic matter maturation of the underlying Woodford Shale. Petrographic analysis suggests that there is no sufficient evidence for hydrothermal alteration in the Sycamore Formation.

1. INTRODUCTION

The Mississippian Sycamore Formation is of interest because it marks deposition during the transition from a sag basin stage to the onset of Pennsylvanian orogenesis (Domeier, 2015), and it records initial stages that marked the closure of the Laurentian and Gondwana plates (Donovan, 2001). The Sycamore Formation also contains a significant economic value as a productive hydrocarbon reservoir especially in recent years as it has been exploited with horizontal drilling and fracture stimulation (Jackson et al., 2018; Miller and Cullen, 2018). In fact, equivalents to the Sycamore Formation have been prolific hydrocarbon reservoirs in the STACK, Merge, and SCOOP plays within the Anadarko Basin and north-central Ardmore Basin (Nojek and Li, 2017; Milad, 2019).

Although there have been studies of the depositional setting of the Sycamore Formation in southern Oklahoma (e.g., Culp, 1961; Franklin, 2002; Milad, 2019), little work has been done on the diagenesis of these rocks. The role that diagenesis plays in terms of reservoir characterization is an open issue that is vital to further produce oil and gas from unconventional reservoirs in the Anadarko and Ardmore Basins. Moreover, fundamental questions about the paragenesis of the Sycamore Formation such as whether the alteration pertains to an open or closed system (e.g., Land et al., 1997; Bjorlykke and Jahren, 2012) remain to be investigated. Results of these studies on the Sycamore Formation could also be important to compare with studies of other units in the Arbuckle Mountains and southern Oklahoma which indicate extensive alteration by basinal (e.g., Elmore, 2001) and hydrothermal fluids (Roberts et al., 2019).

Research has been done on various geoscience subjects in the Sycamore Formation in southern Oklahoma; however, the paragenesis and paleomagnetism of Sycamore rocks are yet to be investigated in detail. No previous study has fully assessed the parageneses of the Sycamore

Formation, especially in outcrop studies. Therefore, this project will attempt to unravel the paragenesis of the Sycamore Formation in order to document the major diagenetic events and understand the controlling factors at a well exposed outcrop along I-35 in southern Oklahoma (Figure 1). The observations will focus on reporting the differences in diagenesis between the major Sycamore lithofacies and recognizing the effects of diagenetic processes on the dynamic evolution of the pore system. After identifying the major diagenetic events, paleomagnetic analysis will be used to test if a magnetization can be used to date the origin of a chemical remanent magnetization (CRM) carried by diagenetic minerals and thereby place an absolute time point into the paragenetic sequence. The principal objectives and hypotheses to be tested in this study are as follows:

1. Determine the paragenesis of the Mississippian Sycamore Formation in outcrop in order to understand the diagenetic evolution between lithofacies and its implications to pore development.
2. Test if diagenetic variations are controlled by lithology (closed system) or regional fluid migration events (open system).
3. Test if hydrothermal fluids have altered the unit.
4. Test if petrofabric analysis can provide a better understanding of particle alignment and level of alteration.
5. Test if a magnetization can be used to determine the timing of diagenetic events and the nature of magnetization (burial or fluid processes).

This project will contribute to the understanding of micro-scale textural fabrics of the Sycamore Formation while adding insights into the diagenetic evolution of Mississippian strata. Applying paleomagnetic studies to date diagenetic events could shed a light onto the complexities

associated with the timing of magnetization, fluid alteration, hydrocarbon migration, fracturing events, and/or maturation of organic matter (e.g., Elmore et al., 2012). This study will also contribute to the understanding of pore development in the Sycamore Formation in the SCOOP play and serve as a future reference for correlations with the Meramec Formation in the STACK play.

1.1. Area of Study

The area of study comprises the Sycamore Formation at the Arbuckle Anticline in southern Oklahoma (Figure 1). The Arbuckle Anticline is one of the most prominent structures in the Arbuckle Mountains as well as the most intensely deformed part of the mountains. It is faulted, asymmetric, and overturned to the north. The Washita Valley fault bounds the northern flank of the Arbuckle Anticline while the Ardmore basin bounds its southern flank (Perry, 1989). With an altitude of approximately 1,377 ft (420 m), the Arbuckle Anticline represents one of the Pennsylvanian-age inversion structures that resulted from the uplift along high angle thrust faults (Miller and Cullen, 2018; Perry, 1989). The evolution of the Arbuckle anticline and its associated minor folds occurred during two major events: (1) the formation of the main anticlinal structure and secondary folds in the Middle Virgilian; and (2) the formation of the Dougherty anticline in the Late Virgilian (Ham et. al., 1969).

The Mississippian exposure along the overturned northern flank of the Arbuckle Anticline (commonly known as the “fried pies outcrop”) dips around 75° to the south-southwest and is located in Murray County, South Central Oklahoma (34°26.780′N, 97°07.839′W). The southern section of the Sycamore Formation (also known as the “I-35 Sycamore outcrop”) is located in Carter County (34°21'3.42"N, 97° 8'54.31"W) dipping southward about 47° into the Ardmore basin. The distance between the two outcrops is approximately 7 miles (Figure 1).

A few comparisons are made with the northern exposure in the course of this project, but the observations and interpretations presented are primarily from the I-35 Sycamore outcrop which is an excellent 450 ft exposure of the complete Sycamore Formation. From its basal contact with the Woodford Shale to the overlying Caney Shale, the southern Sycamore section is much thicker than the northern overturned exposure (221 ft as recorded by Fay, 1989).

2. GEOLOGIC SETTING

2.1. Regional Structure

The oldest structural events identified in the Anadarko Basin region are associated with crustal consolidation across Laurentia and regional high-grade metamorphism during the Precambrian time (Perry, 1989). The subsequent development of a failed arm or linear rift of a triple junction occurred in southern Oklahoma between the late Precambrian to the middle Cambrian time. The three radial arms continued to spread and formed a continental rift zone; however, the NW-trending arm failed and extended into the continent as an aulacogen (Franklin, 2002). The aulacogen is now commonly termed the Southern Oklahoma Aulacogen (SOA). Its evolution includes three different stages to reach its final configuration: (1) rifting, (2) subsidence and infilling of the rift, and (3) rock deformation (Cole, 1988).

The rifting stage began during late Proterozoic and consisted of uplift, extensional rifting, faulting, and the development of grabens as well as small rift valleys. This stage was also characterized by extensive igneous activity along the axis of the Southern Oklahoma Aulacogen. The Cambrian Colbert Rhyolite present in the center of the Arbuckle Anticline serves as evidence for the rifting stage of the SOA (Franklin, 2002). At the end of the rifting stage, the aulacogen began to cool and subside resulting in the formation of the southern Oklahoma trough (Perry, 1989). From the Cambrian to early Mississippian time, the southern Oklahoma trough established

a principal axis of sedimentation parallel to the northwest-southeast trend of the aulacogen (Caylor, 2019).

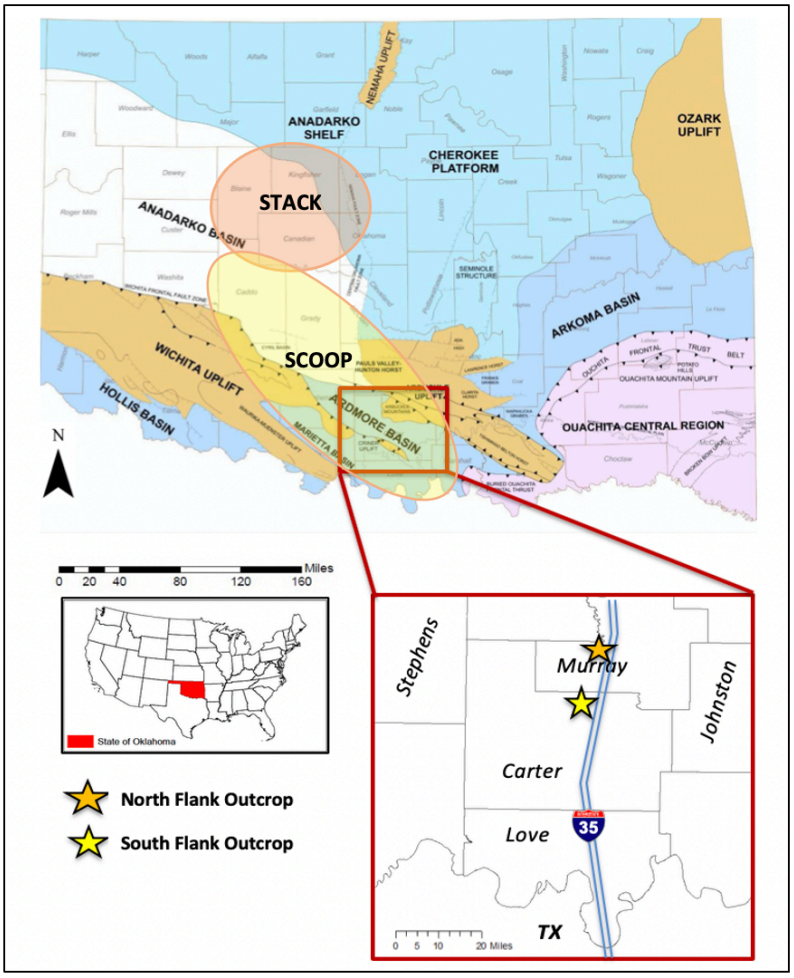

Figure 1. Map outlining the location of the study area in the Ardmore Basin, Southern Oklahoma. The yellow star indicates the location of the southern flank of the Arbuckle Anticline which represents the complete exposure of the Sycamore Formation (Interstate 35 highway outcrop or "I-35 Sycamore outcrop"). The samples for this study were collected in the South Flank section; however, the green star indicates the Sycamore exposure in the North Flank of the Arbuckle Anticline for reference and comparison. The distance between the two outcrops is approximately 7 miles. The delineated orange area represents the STACK play while the yellow area represents the SCOOP play. (Modified from Northcutt and Campbell, 1998).

The subsiding stage of the SOA was the longest stage ranging from late Cambrian to Mississippian time (Franklin, 2002). Rapid subsidence created sufficient accommodation space to allow the deposition of a very thick sedimentary sequence (Ham et. al., 1969). Approximately

34,000 feet of sediment was deposited in the SOA, and those that accumulated in the Anadarko Basin attest to the subsidence stage of the Southern Oklahoma Aulacogen (Palladino, 1985). In addition to thick sediment accumulation, the subsidence stage was also accompanied by the formation of a passive continental margin and a marine transgression which eventually played a significant role in Sycamore deposition (Allen, 2000; Franklin, 2002).

The final deformation stage was marked by the reactivation of faults originated during the rifting stage and the development of orogenic structures. The Laurentia-Gondwana collision during the Late Pennsylvanian caused extensive deformation of the aforementioned thick sedimentary package followed by tectonic uplifts such as the Wichita, Ouachita, and Arbuckle Mountains (Perry, 1989; Granath, 1989; Franklin, 2002). Progressive deformation in the foreland of the Ouachita orogeny led to the development of the structurally complex Ardmore Basin. Structural inversion associated with the Laurentia-Gondwana collision resulted in the growth of the asymmetric Anadarko Basin which experienced minimal structural deformation since the Permian time (Perry, 1989; Granath, 1989). The Arbuckle Anticline (Figure 2) is one of various Pennsylvanian-age inversion structures that segmented the Southern Oklahoma Aulacogen into a series of foreland basins: Ardmore, Anadarko, Arkoma, Marietta, and Forth Worth (Miller and Cullen, 2018).

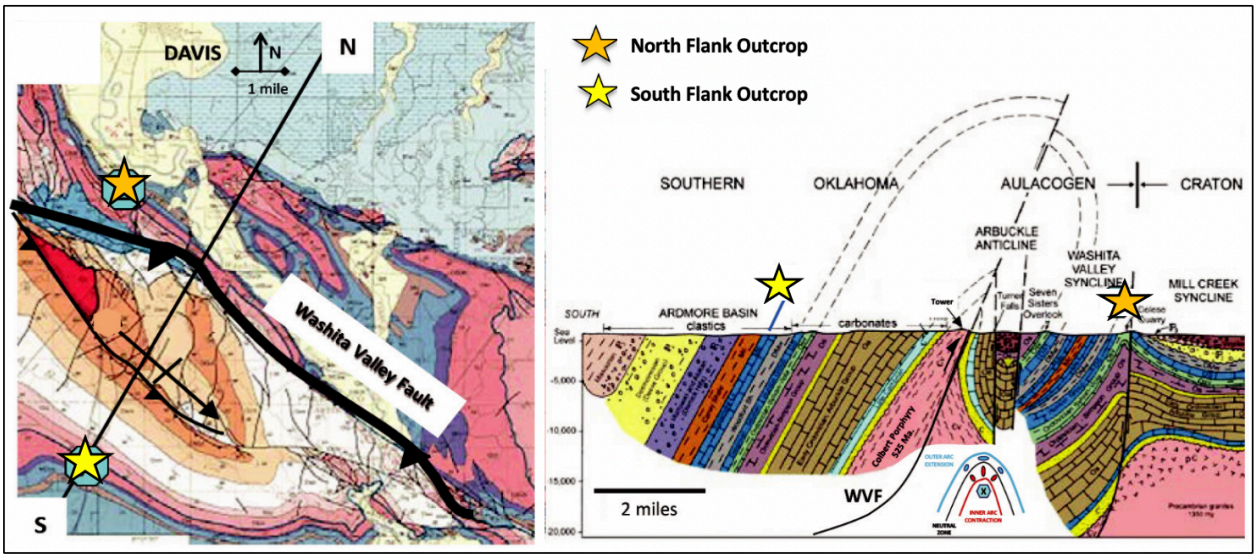

Figure 2. (Left): Geologic map of the Arbuckle Mountains (Ham et al., 1954; revised by Johnson, 1990) depicting the location of Sycamore exposure and the profile line for the cross section. (Right): Cross sectional view of the Arbuckle Anticline in southern Oklahoma (Ham and McKinley, 1954; revised by Johnson, 1990). Modified from (Miller and Cullen, 2018).

2.2. Stratigraphy

The regional stratigraphy of this area is a reflection of the processes associated with the evolution of the Southern Oklahoma Aulacogen. In fact, the rock units deposited during the Upper Devonian to Middle Mississippian represent periods of significant subsidence in the aulacogen (Franklin, 2002). The stratigraphy of the study area consists of Sycamore rocks overlying the Upper Devonian to Early Mississippian Woodford Shale, and Chesterian series sitting on top of the complex Sycamore Formation (Figure 3).

During Mississippian time, a large and tropical epicontinental sea (Figure 4) covered part of North America landmass (Curtis and Champlin, 1959) and this vast sea continued to extend throughout the Midcontinent area (Northcutt, et al., 2001). As a result, the Sycamore Formation was deposited in the Southern Oklahoma Aulacogen on the shelf to the north during the major marine transgression in Meramecian time (Schwartzapfel, 1990). Earlier studies suggested that the Sycamore Formation was deposited in relatively shallow water followed by reworking due to waves and local currents (Champlin, 1959; Cole, 1988). However, later on, Schwartzapfel (1990)

and Coffey (2000) proposed a depositional mechanism associated with turbidity currents or gravity flows justifying the transport of sediments into such a low energy environment. Recent studies claimed that the Sycamore Formation was deposited on a slope setting as gravity flows or below a storm wave base. The presence of carbonate grains is attributed to deep surface or bottom surface currents (Franklin, 2002; Miller and Cullen, 2018; Milad, 2019).

The Mississippian carbonates of the northern Anadarko Basin were deposited on a stable shelf and ramp setting which moved down-dip into the deep-water siltstones and mudstones of the Osage, Meramec, and Sycamore formations (Terrel, 2019). The Sycamore Formation in the SCOOP (South Central Oklahoma Oil Province) play is coeval with the Meramec Formation of the STACK (Sooner Trend Anadarko Canadian Kingfisher) play (Figure 1). A depositional sequence of argillaceous to calcareous siltstones comprises the primary facies of the Meramec Formation, and a series of depositional, physiochemical, and tectonic factors justify the lateral variations of facies in Mississippian rocks in Oklahoma. The Meramec Formation consists of shallowing upward cycles capped by marine-flooding surfaces deposited in systems of low-angle clinoforms reworked by currents within or below storm wave base (e.g., Miller, 2018; Price et. al., 2020).

The Sycamore Formation consists of a mixed carbonate siliciclastic system (Duarte, 2018; Milad, 2019) resulted from turbidity currents and gravity flows that developed incomplete Bouma sequences, contorted bedding, and flute casts (Terrel, 2019; Milad, 2019). Terrel (2019) concluded that the Osage in the STACK is the time equivalent of the Lower Sycamore Formation in the SCOOP whereas the Meramec in the STACK is the time equivalent of the upper portions of the Sycamore Formation in the SCOOP. Terrel (2019) also added that the Sycamore “Limestone” derived from a northern (Osage) and southern sediment source.

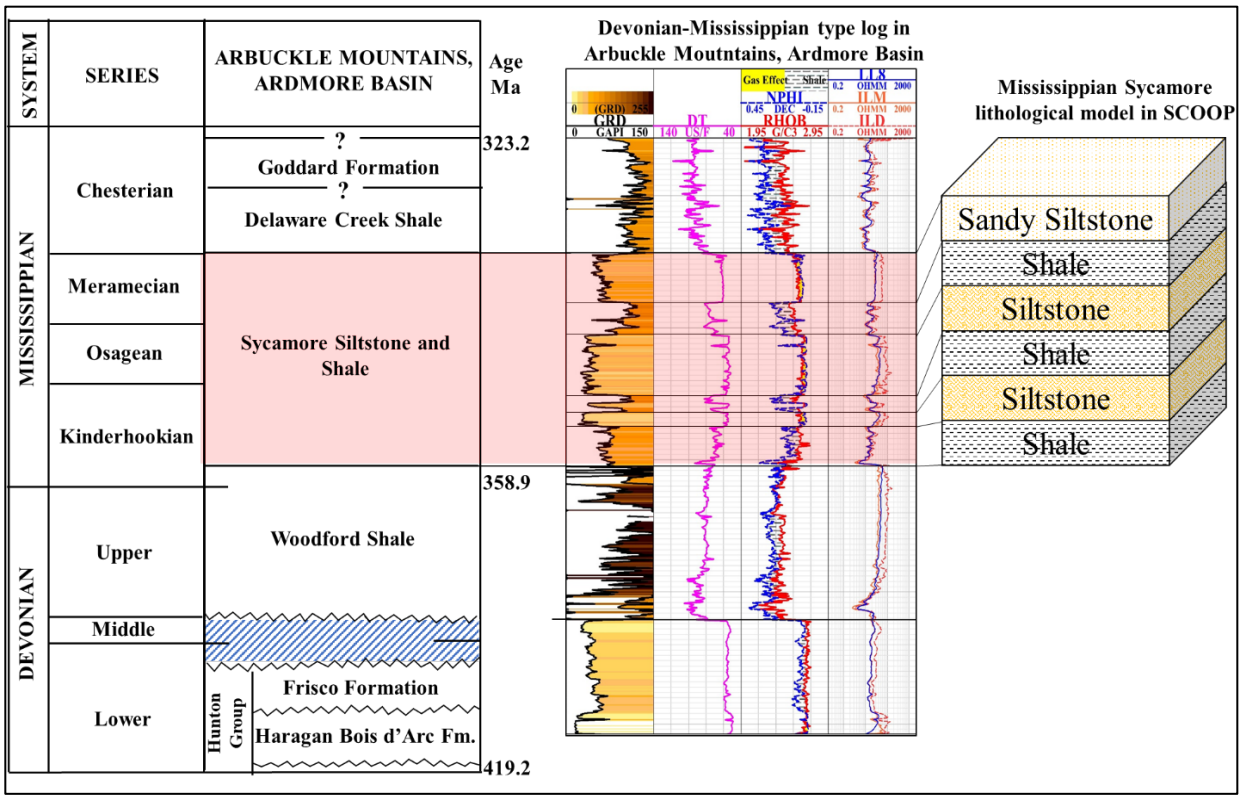

Figure 3. Representative Mississippian stratigraphic column of the Arbuckle Mountains originally modified from (Johnson and Cardott, 1992). However, Milad (2019) modified the nomenclature of the "Sycamore Limestone" to account for the new observations which classify the system as siliciclastic rather than entirely carbonate. Note that the Woodford Shale underlies the Sycamore Formation, which is capped by the Delaware Creek Shale, also known as Caney Shale. Milad (2019) also combined the Devonian-Mississippian type-log to illustrate the subsurface pattern of the Sycamore Formation with emphasis on the significant changes in the Gamma Ray log.

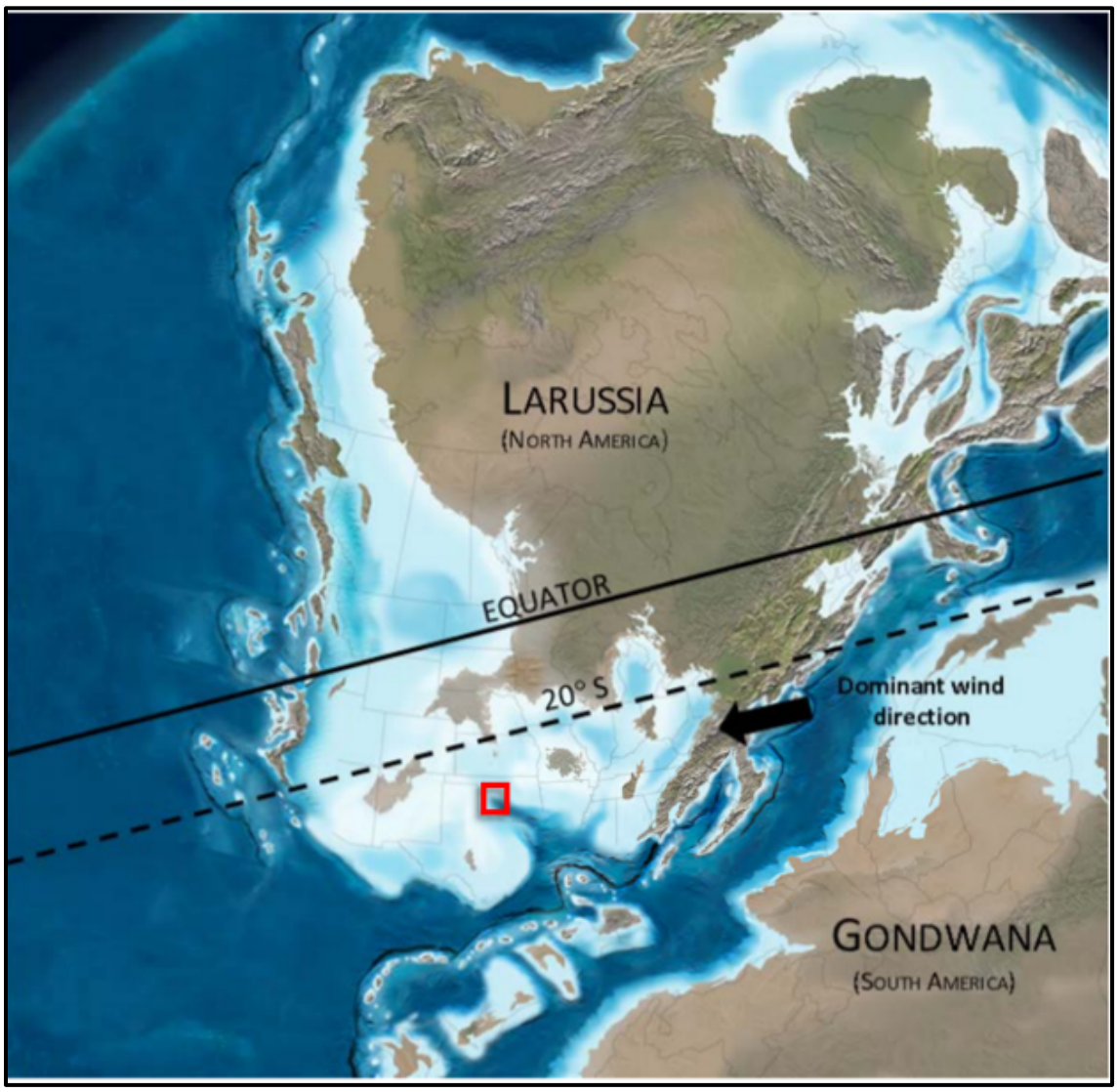

Figure 4. Paleogeographic map of the early Mississippian time (358 Ma). The area highlighted in red illustrates the study area which was covered by a shallow sea prominent in the North America landmass. The prevailing wind was from the present-day northeast direction. (Modified from Blakey, 2013 and Terrel, 2019).

At the I-35 outcrop (Figure 5), the contact between the Woodford Shale and Mississippian units is very evident as the rocks transition from chert beds with phosphate nodules to a green fissile shale. Field observations from Milad (2019) suggest six stratigraphic sections within the I-35 Sycamore outcrop, namely: Lower Shale Transition Section (LShTS); Lower Sycamore Section (LSyS); Middle Shale Section (MShS); Middle Sycamore Section (MSyS); Upper Shale Section (UShS); and Upper Sycamore Section (USyS). With these distinctive subdivisions, the same

nomenclature will be utilized throughout this research alongside to the outcrop lithofacies established by Milad (2019).

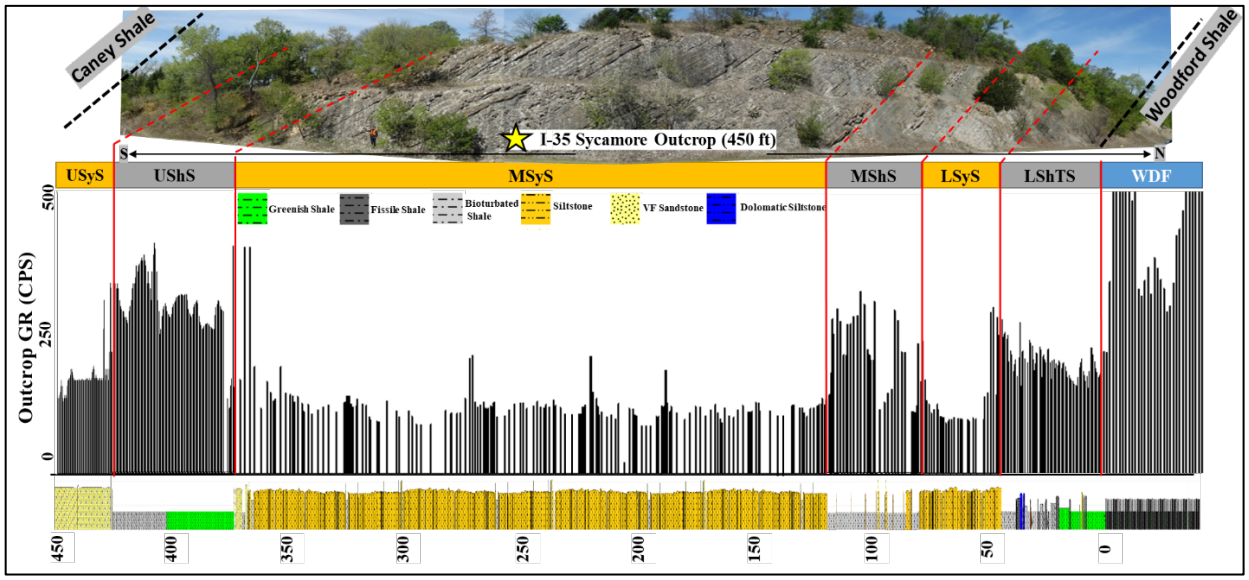

Figure 5. Cross-sectional view of the I-35 Sycamore outcrop depicting the stratigraphic sections defined by Milad (2019). The up-section direction is from North (right side) to South (left side). The illustration at the bottom represents outcrop Gamma Ray readings in counts per second; note the high radioactive pattern in the Upper Shale Section (UShS). Modified from (Milad, 2019).

3. PREVIOUS STUDIES

3.1. Lithostratigraphic and Chronostratigraphic Studies

Numerous studies have been done in the Sycamore Formation, and the earlier studies focused mainly on the stratigraphy and the age of the formation (e.g., Taff, 1903; Cooper, 1926; Prestridge, 1957). Between 1961 and 1987, there were some large-scale outcrop work and publications that referred to the Sycamore Formation, but none of these studies analyzed it in detail nor determined its actual age (e.g., Fay, 1989). In 1988, Cole published his work on the Sycamore "Limestone" by defining six formation lithofacies and suggesting a lagoonal or slightly deep marine environment of deposition; however, there were still arguments regarding the chronostratigraphic position of the Sycamore Formation. Schwartzapfel (1990) observed conodont

elements typical of Upper Mississippian at the very top of the Woodford Shale at the southern flank of the Arbuckle Anticline (I-35 outcrop). Through conodont zonation studies, these observations suggested that the Sycamore Formation could not be older than the Middle Meramecian in age. Therefore, Schwartzapfel (1990) concluded that the lower Sycamore is not older than middle Meramecian while the upper Sycamore is upper Meramecian to lower Chesterian in age. He also concluded that the upper Sycamore is partially "turbiditic in origin" due to the occurrence of an incomplete Bouma Sequence indicative of deep-water environments.

Donovan (2001) performed a meticulous field study comparing and contrasting the two Sycamore sections in the Arbuckle Mountains, Oklahoma. With emphasis primarily on facies interpretation and petrography, Donovan (2001) recognized two members in the Sycamore Formation: (1) gray shales and argillaceous limestones constituting the lower "transition" member; (2) interbedded gray shales and tan-weathering marlstones containing significant silt-sized siliciclastic grains which comprise the upper member. Donovan (2001) established two main lithologies in the Sycamore Formation: gray shales and limestones/marlstones. There is little difference in the mineralogy and texture of the beds between the two Sycamore sections; however, single beds are usually thicker in the northern overturned section than in the southern exposure. Perhaps these differences are due to stratigraphic variations and/or structural thinning during overturning of the beds in the northern section.

Regarding depositional settings, Donovan (2001) reported that the sedimentary structures in individual beds are not characteristic of a particular environment. But as a whole, it seems that the beds record "rapid deposition" from a mass gravity flow deposit which is somewhat similar to Schwartzapfel's (1990) depositional model. Settling grain fabrics and disruptive bioturbation observed in thin sections supports the hypotheses that the bulk of the Sycamore Formation was

deposited rapidly under “fluidized (turbidity) flow conditions”. Donovan (2001) also added that the carbonate grains in the Sycamore Formation attest to the existence of a carbonate shelf to the north while the siliciclastic grains suggest that tectonic uplift occurred at some distance to the east and north.

Deciphering the depositional conditions of the Sycamore Formation can be challenging because the literature offers different depositional environment interpretations. Some studies suggest deposition in shallow water transgressive conditions (Bennison, 1956; Prestridge, 1957; Cole, 1988) while others propose deposition on a slope or below storm wave base setting (Schwartzapfel, 1990; Franklin, 2002; Miller and Cullen, 2018). However, most of these aforementioned studies presented depositional environment interpretations without conducting a detailed rock characterization and lithofacies classification of Sycamore strata.

Milad (2019) published one of the most recent studies on the Sycamore Formation (I-35 outcrop) consisting of detailed lithofacies characterization and in-depth field work aiming to unravel the formation’s depositional history. The study divided the I-35 Sycamore outcrop into six stratigraphic sections and seven lithofacies which are heavily referenced in the course of this project. Milad (2019) attributed the presence of pyrite crystals, chert beds, and high radioactivity as an indicative of deep-water conditions for the siliceous shale facies in the Sycamore Formation. On the other hand, the occurrence of Bouma Sequence (Ta-Te) in the Sycamore siltstone strongly suggests deposition by slope gravity flow processes. These interpretations are accordant with earlier observations suggesting Sycamore deposition in a slope setting or below storm wave base/deep waters (Schwartzapfel, 1990; Donovan, 2001; Franklin, 2002; Miller and Cullen, 2018), and it seems that it is currently the acceptable depositional model for Sycamore rocks.

3.2. Diagenetic Studies

After multiple chronostratigraphic studies (e.g., Culp, 1961; Cole, 1988; Schwartzapfel, 1990), researchers began to take a different approach in understanding the complexities of the Sycamore Formation. Coffey (2000) agreed with Schwartzapfel's (1990) chronostratigraphic position and depositional interpretation of the Sycamore Formation, and he was one of the pioneers attempting to understand the diagenetic history of the Sycamore Formation with emphasis on reservoir characterization in the Carter-Knox Field.

According to Coffey (2000), past tectonic activity had a significant impact on reservoir quality of the Sycamore Formation in Carter-Knox Field. The extensive periods of uplift and successive meteoric diagenesis produced porosity values characteristic of this field. Coffey (2000) added that calcite is the primary cement of Sycamore facies and that undersaturated fluids leached the calcite, creating secondary porosity and enhanced permeability in the high-relief areas of the field. His observations did not present sufficient evidence to explain the pre-diagenetic factors defining the course of diagenesis and the role of fractures or mineralization in the Sycamore Formation. Furthermore, Coffey's (2000) study lacks a paragenetic sequence documenting the sequential order of mineral phases. Coffey's (2000) research only focused on integrating subsurface data to unravel the depositional history of the Sycamore Formation while also assessing aspects of the diagenetic history.

Several studies have investigated the Mississippian strata regionally and in north central Oklahoma. For example, Dehcheshmehi et. al., (2016) completed a regional diagenetic study on the Mississippian strata of the southern Midcontinent with the aim of understanding the effects that basinal fluids had on reservoir quality. The study revealed that the principal diagenetic events affecting these rocks occurred during burial and basinal fluid migration through these units.

Amongst several observations, the study claimed that late diagenetic calcite and quartz cements fill the fractures, breccias, and vugs in Mississippian carbonate facies in north-central Oklahoma. Stable isotope data indicates that these fractures are coeval with regional flow of saline basinal fluids associated with orogenic events such as the Ouachita tectonism (Dehcheshmehi et. al., 2016).

Following the regional study presented by Dehcheshmehi et. al., (2016), Duarte (2018) introduced an integrated study characterizing the Mississippian strata in central Oklahoma with emphasis on the Meramec Formation. After detailed core descriptions, thin section analysis, scanning electron microscopy (SEM), and X-Ray fluorescence (XRF) interpretations, the study suggested two facies associations to the Meramec Formation- gravity flows and hemipelagic sediments. Additionally, the study revealed that the occurrence of blocky calcite cement in the Mississippian strata depends on diagenetic processes controlling reservoir quality. The blocky calcite cement is believed to occlude primary porosity and it was precipitated during burial late diagenesis (early to middle stages) in the calcite-cemented siltstones of the gravity flow facies (Duarte, 2018). Nonetheless, Hardwick (2018) highlighted the primary pore types present in the Meramec microfacies including dissolution pores in feldspars, interstitial pores in clay, and intergranular pores among framework grains. With that, interstitial clay porosity is common in the argillaceous siltstone facies while the porosity associated with dissolution of unstable grains is abundant in the calcareous siltstones (Hardwick, 2018).

Terrell (2019) published one of the most recent studies on the diagenetic characterization of Mississippian rocks. His work mainly addressed the extent to which diagenetic alteration affects reservoir quality. Similar to Duarte (2018) and Hardwick (2018), Terrel (2019) agreed that marine calcite cements occlude primary porosity within the siltstone facies in the Meramec and Sycamore

Formations. Though porosity in the Sycamore Formation is primarily enhanced as a result of meteoric diagenesis, increasing clay content prevents calcite nucleation and therefore, preserves primary porosity. Although Duarte (2018), Hardwick (2018), and Terrell (2019) presented a more detailed diagenetic interpretation compared to Coffey (2000), their studies assessed diagenesis in cores combined with a series of subsurface, geochemical, and paleomagnetic data. Therefore, there is still a necessity for assessing the parageneses of Sycamore rocks in outcrop and understanding its diagenetic evolution.

3.3. Paleomagnetic Studies

Paleomagnetism of Sycamore rocks is yet to be investigated in detail, though analyzing the timing and origin of fluid migration events in the Arbuckle Mountains has been subject of active research for a number of years (e.g., Elmore, 2001). The dating method consists of isolating the chemical remanent magnetization (CRM) carried by authigenic minerals that precipitate during rock-fluid interactions and comparing the pole position from the CRM with the position in the Apparent Polar Wander Path (APWP) (Elmore et al., 1998). In addition to determining the timing of remagnetizations, paleomagnetic studies are also critical to discern the extent and timing of fluid alteration relative to hydrocarbon migration, fracture events, and maturation of organic matter.

Numerous paleomagnetic studies have taken place in the Midcontinent area (e.g., McCabe and Elmore, 1989; Elmore et al., 1998; Elmore et al., 2012; Heij, 2018; Roberts et al., 2019), and most interpretations suggested that hydrothermal alteration plays a major role in mechanical properties and reservoir quality of Mississippian rocks in Oklahoma. Elmore et al. (2017) documented evidence of Permian remagnetization of Mississippian Carbonates in north central Oklahoma as a result of hydrothermal fluid flow events. Dehcheshmehi et. al., (2016) claimed that deeper basin fluids associated with the Ouachita and Appalachian orogenies might have

diagenetically altered the Meramec facies in the STACK play. Furthermore, Hardwick (2018) found a characteristic remanent magnetization (ChRM) in the Meramec which implies hydrothermal alteration and/or association with the emplacement of hydrocarbons. With that, testing for secondary magnetizations in the Sycamore Formation and ultimately correlating the results with previous observations in the Meramec Formation can provide a better understanding of diagenetic events and perhaps develop a temporal component on the evolution of the petroleum system.

4. METHODOLOGY

4.1. Petrography

Petrographic analysis was conducted on a total of thirty-seven thin sections from the Sycamore Formation in both the southern and northern flanks of the Arbuckle Anticline. Core plugs were sampled from the I-35 Sycamore outcrop for thin section preparation which resulted in thirty-three thin sections (Figure 6). These thin sections covered the entirety of the I-35 Sycamore outcrop and they were selected based on the representative outcrop facies and distinctive features such as mineralized fractures. Due to field sampling constraints, only four thin sections were sampled from the northern flank Sycamore exposure ("fried pies" outcrop), mainly for comparative purposes. The thin sections were impregnated with blue epoxy and polished to a thickness of thirty microns. Some thin sections were stained with alizarin red S (ARS) with the aim of distinguishing between calcite and dolomite grains.

Optical microscopy was performed under cross-polarized, plane-polarized, and reflected light on a Zeiss AxioImager.Z1m. The photomicrographs were captured with a linked AxioVision microscope camera attachment. The thin section analysis assisted in organizing each thin section into a microfacies classification scheme in order to characterize the variability of diagenetic alteration within the study area. The microfacies classification was based on composition, sorting, grain size, and volume proportion of cements, framework grains, matrix, and authigenic phases. The estimation of mineral volume proportion was solely done through petrographic observation since quantitative mineral volume determinations via point counting were not performed. The paragenetic sequence was constructed based on cross-cutting and textural relationships.

A FEI Quanta 250 Scanning Electron Microscope (SEM; BSE – backscattered electron imaging, SE – secondary electron imaging) with a Bruker Electron Dispersive Spectrometer (EDS)

was utilized to image and identify micron scale diagenetic minerals and features. Ten thin sections were selected for SEM analysis and they were covered with gold to prevent chemical charging during electron beam exposure. The microphotographs were taken by using the Everhart Thornley Detector and (ETD) and Circular backscatter detector (CBS) at specific operating conditions. SEM analysis was vital to quantify elemental analysis of mineral phases and provide supplemental micro-scale observations.

4.2. Paleomagnetism

A total of ninety-two core plug samples were collected from the outcrops on both the northern and southern flanks of the Arbuckle Anticline. Eighty-two samples were collected from nine different sites covering the entirety of the southern flank Sycamore exposure (Figure 6). However, only a total of ten core plugs were collected from the north flank Sycamore exposure due to the limited access to suitable beds for drilling and extensive vegetation. Data from seven samples from the Woodford Shale exposure in the I-35 outcrop and eight samples from the south flank of the Sycamore I-35 outcrop that were collected as part of previous class projects were also analyzed. The core plug samples were collected using a portable gas-powered drill and oriented using a Brunton compass attached to a clinometer. The oriented cores were then cut into a standard plug size (2.5 cm diameter X 2.2 cm height) by using a water-cooled drill press.

A total of twenty-five samples were subjected to two demagnetization techniques - alternating field (AF) and thermal demagnetization. One specimen from each flank of the Arbuckle Anticline was subjected to a pilot alternating field (AF) demagnetization up to 120 millitesla (mT) in 10 mT increments. Sixteen specimens from the southern flank underwent stepwise, thermal demagnetization in 20-50°C increments up to 500°C. The seven specimens from the Woodford Shale underwent AF demagnetization up to 100 mT in 10 mT increments. The natural remanent

magnetizations (NRM) were measured using a 2G Enterprises three-axis cryogenic magnetometer with DC SQUIDs (superconducting quantum interference device) located in a magnetically shielded room. Data processing and interpretation was performed in the SuperIAPD program by picking principal components on orthogonal projections (Zijederveld, 1967) of inclination and declination values. After performing principal component analysis (Krischvink, 1980), the magnetic components with mean angles of deviation (MAD) less than 18° were used to calculate mean statistics (Fisher, 1953).

4.3. Anisotropy of Magnetic Susceptibility

Low-field anisotropy of magnetic susceptibility (AMS) was determined to assess the magnetic petrofabric of the Sycamore Formation. Seventy-two core plugs were collected from a total of nine sites in the Sycamore I-35 outcrop (Figure 6) and the cores were cut to the dimensions of standard AMS specimens (2.5 cm diameter X 2.2 cm height). The AMS was measured using a KLY-4S Kappabridge magnetic susceptometer and the data was processed using Anisoft 4.2 (Chadima and Jelinèk, 2009). The magnetic susceptibility represents the degree of magnetization (M) of a material in response to an applied magnetic field (H). The AMS is represented by an ellipsoid with three mutually perpendicular principal axes K1 (maximum), K2 (intermediate), and K3 (minimum). The shape of the ellipsoid can be described by the shape parameter (T) where an

oblate magnetic fabric is observed when $0 \leq T \leq 1$ and prolate when $-1 \leq T \leq 0$ (Jelinèk, 1981). A normal magnetic fabric occurs when the principle magnetic axes (K1, K3) coincide with crystal shape axes (e.g., phyllosilicates) or inverse, where the K1 parallels the foliation and K3 parallels the lineation (e.g., ferroan dolomite) (Rochette, 1987). Moreover, a combination of inverse and normal magnetic fabrics is known as mixed/intermediate fabrics (Ferré, 2002).

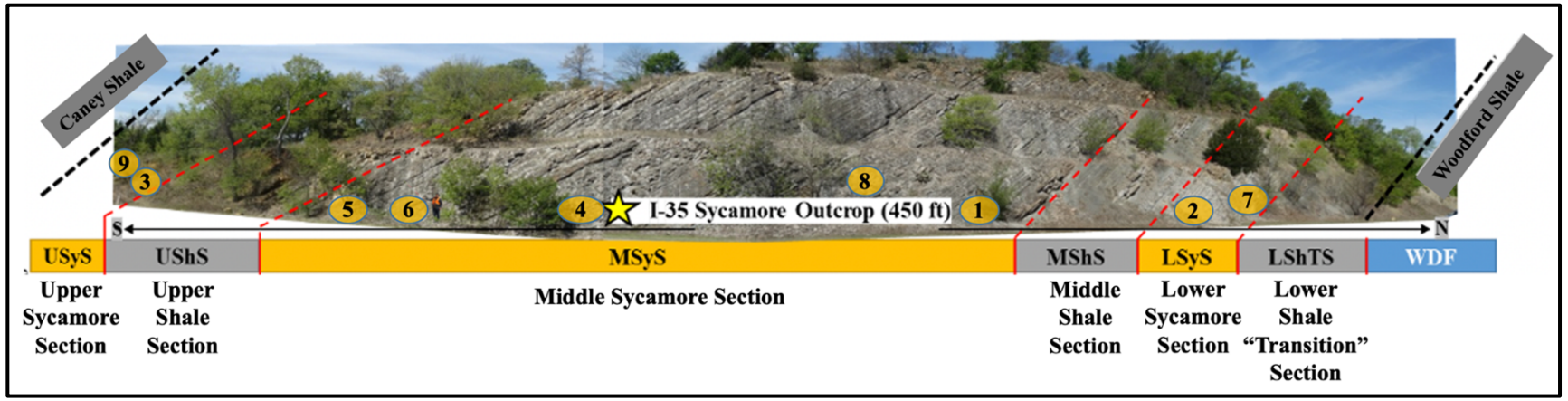

Figure 6. Photomosaic of the I-35 Sycamore Outcrop from its northern contact with the Woodford Shale through its southern contact with the Caney Shale. The numbers indicate site location for core plug sampling. These core plugs were used for thin section preparation, thermal demagnetization, and anisotropy of magnetic susceptibility measurements. (Modified from Milad, 2019).

5. RESULTS AND INTERPRETATIONS

5.1. Microfacies Classification and Description

Petrographic analysis reveals three major lithologic groups in the Sycamore Formation: clay-rich mudrocks, silt-rich mudrocks, and carbonate-rich mudrocks. Following Lazar et al.'s (2015) rock classification scheme, the lithologic groups are subdivided in five predominant microfacies based on grain size and composition of major mineral fraction (detrital, biogenic, and authigenic phases). The five microfacies include argillaceous mudrock, siliceous mudrock, calcareous mudrock, calcitic siltstone, and calcite-cemented siltstone. The argillaceous, calcareous, and siliceous mudrock microfacies were observed in samples from the Sycamore Shale member whereas the calcitic siltstone and calcite-cemented facies were observed in the Sycamore Siltstone member, also widely held as Sycamore "Limestone".

Sycamore Mudrock Microfacies

The argillaceous mudrock microfacies (Figure 7A) are clay-rich (~50%) with a dark clay matrix, quartz-silt grains (~30%), and detrital organic matter. Silica components occur as sub-angular to angular quartz-silt with grain sizes ranging from 0.0078 to 0.0156 millimeters (mm). In addition to the presence of detrital quartz in the matrix, biogenic silica in the form of radiolarians and other palynomorphs such as tasmanites are also observed in this microfacies. The majority of the palynomorphs appear flattened or collapsed creating parallel preferential alignments along thinly laminated layers. Silica replacement of fossil fragments and local clay partings associated with the depositional structure of clay minerals are common within the matrix. Carbonate mineral phases are present in small amounts (~7-10%), possibly as calcite cement, but its low concentration might be due to the fact that the primary pore space where calcite would potentially precipitate might have been occluded by clay particles. Little to no porosity is observed at the petrographic

microscope scale; however, SEM analysis reveals interstitial porosity associated with the clay structure in the matrix and organic-matter pores (Figure 8A). Pyrite crystals appear dispersed throughout the matrix in the form of cubic crystals and framboids. Euhedral pyrite crystals appear to have replaced some allochems such as radiolarians and Tasmanites; however, prior to pyritization, these allochems are typically replaced by a form of silica. Mineralized fractures are not observed in this microfacies.

The siliceous mudrock microfacies are characterized by a matrix with a mixture of microcrystalline quartz, calcite, muscovite, and clay particles (Figure 7B). Sub-angular to angular quartz-silt grains are the principal components of this microfacies (~50%) though carbonate material is also predominant (~35%) in the form of calcite cement and minor dolomite rhombs. The detrital silt-sized quartz appears isolated in the matrix as well as scattered in thin lenses. Argillaceous material occurs both in the matrix (~10%) and as clay laminations, commonly with a contorted geometry. On a microscope scale, flat grains such as muscovite flakes can be bent or deformed between quartz and calcite grains. Organic material is unevenly distributed as patches not aligned in preferential planes. Soft-sediment deformation and burrowing occur in the siliceous-rich facies. Pyrite is commonly observed as cubic crystals or framboids replacing portions of organic materials. Radiolarians are rare, but flattened tasmanites and agglutinated forams are observed as coarser silicified grains in the matrix.

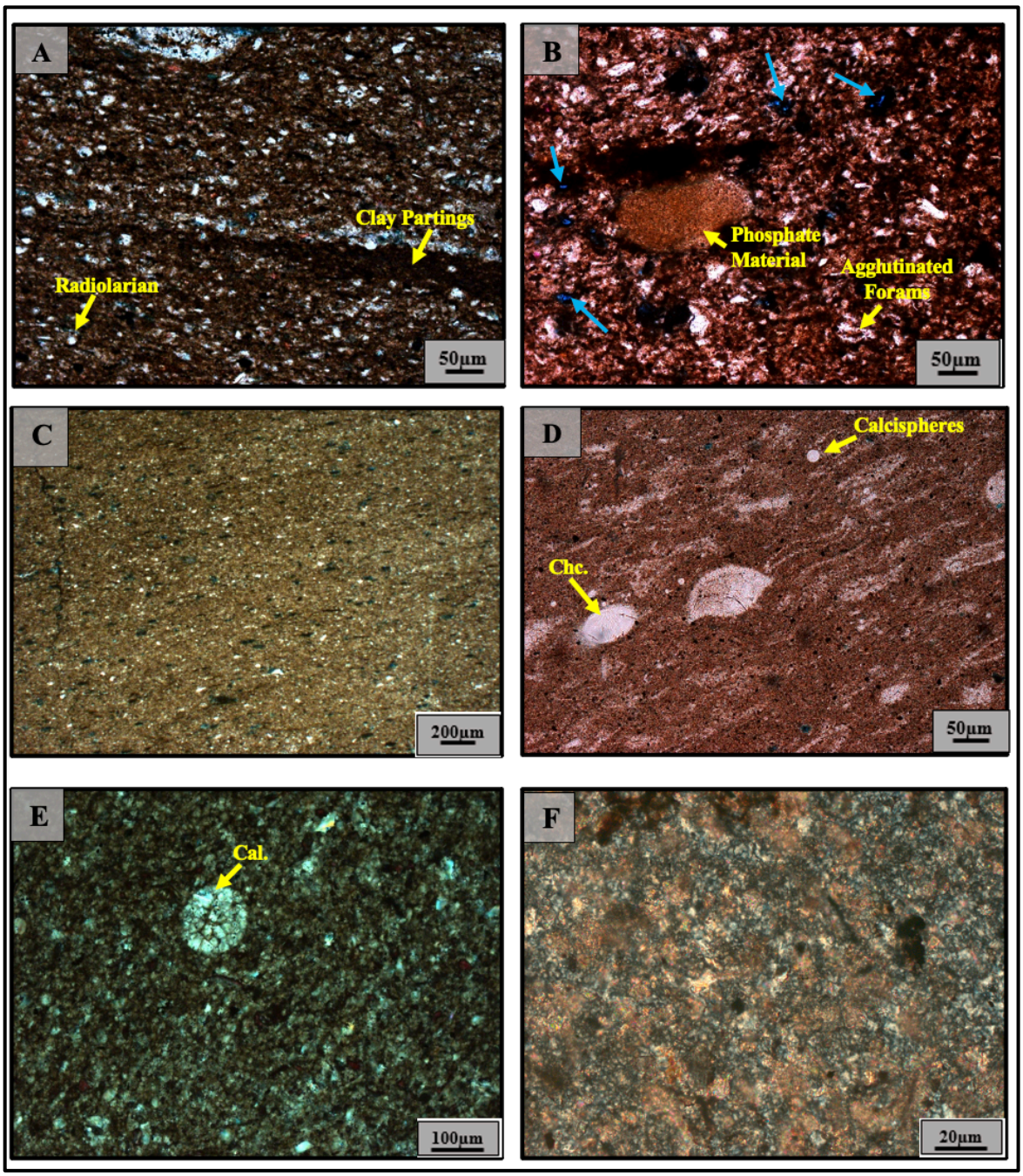

Figure 7. Representative microfacies of Sycamore mudrocks. Plane polarized light (PPL) photomicrographs. **A)** Argillaceous mudrock showing a dark clay matrix with detrital silica, biogenic silica in the form of radiolarians, and authigenic silica replacing fossil fragments. **B)** Siliceous mudrock with large phosphate grains. Calcite is stained red. Blue arrows indicate the intergranular pore spaces. **C)** Calcareous mudrock with a fine grained micritic matrix. **D)** Calcareous mudrock with abundant clay content and replacement of microfossils by chalcedony. **E)** Calcareous mudrock with fine grained micritic matrix and large calcispheres. **F)** Calcareous mudrock with a coarser crystalline matrix and sparry calcite cement.

Additional minerals in the siliceous mudrocks include gypsum (<2%) and large early diagenetic grains (up to 250 µm in diameter) of phosphate material (~3%) (Figure 7B). Phosphate concretions have been documented in outcrop studies in the I-35 exposure, particularly in the Uppermost Woodford section (Figure 6) which marks the contact with the Lower Transition Shale Section (LTShS) in the Sycamore Formation (e.g., Galvis, 2017). Microscopic analysis of the LTShS samples shows abundant detrital grains of phosphate material which could possibly be collophane grains as seen in the siliceous mudrock microfacies. Intergranular pores were observed around mineral grains over a wide range with uneven distribution, typically in spaces associated with organic material and clay aggregates.

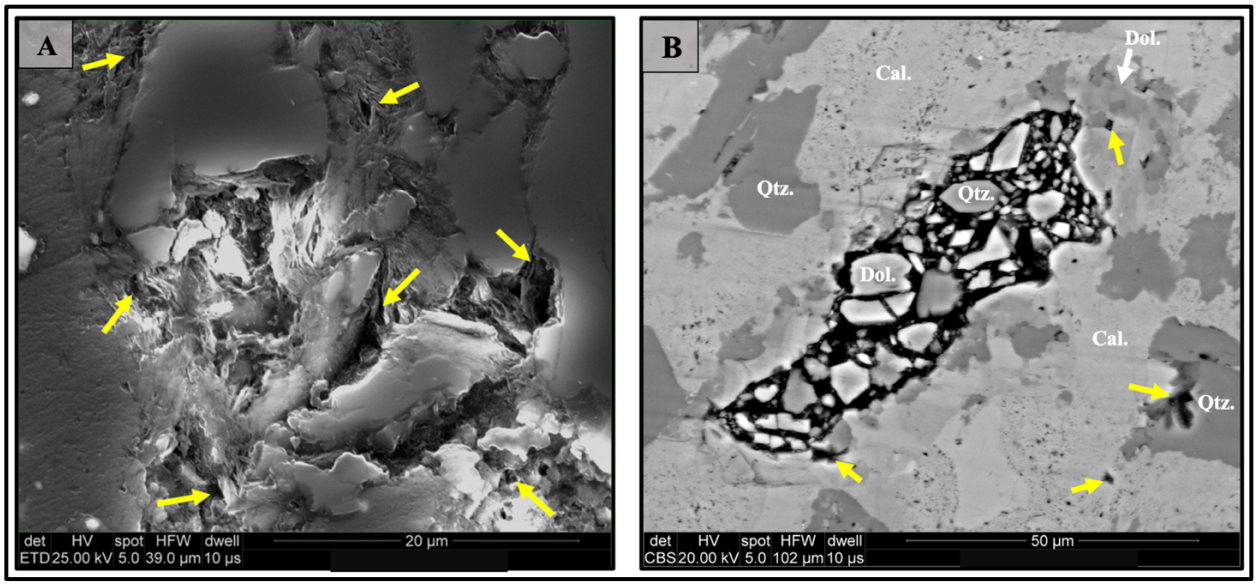

Figure 8. Common pore-types within Sycamore mudrocks. Backscatter SEM images. **A)** Interstitial porosity associated with the clay structure in the matrix and organic-matter pores in argillaceous mudrock microfacies. Yellow arrows indicate pore spaces. **B)** Large dissolution vug filled with dolomite (Dol.), quartz (Qtz.), and dissolved calcite grains (Cal.). Yellow arrows indicate intergranular porosity and possible pores within vugs.

In the calcareous mudrock microfacies (Figure 7C-F), the textures of carbonate components vary significantly. Calcareous mudrock samples from the Lower Transition Shale Section (LTShS) and Lower Sycamore Section (LSyS) predominantly consist of a micrite matrix

with calcite cement (~70%), detrital quartz-silt (~10%), framboidal and cubic pyrite (~5%), barite (~3%), and amorphous dark material (~2%) (Figure 7C). Allochemical grains such as peloids are relatively common and low amounts of biogenic silica are observed in the form of discrete radiolarians within the matrix. Calcispheres and circular grains of carbonate nature (Figure 7E) are sporadically distributed in the calcareous mudrock microfacies with fine-grained carbonate mud. In the Middle Sycamore Section (MSyS), the calcareous mudrock microfacies contain a carbonate matrix with less micrite but increasing amounts of a coarser crystalline calcite matrix (sparite) and sparry calcite cement (Figure 7F). Groups of microfossils aligned in a preferred orientation occur as lenses filled with calcite and/or silica-rich crystals around the rims. In other instances, microfossils are filled with micro-fibrous chalcedony cement (Figure 7D) replacing the original carbonate composition. The presence of lobate edges and embayments in some microfossils suggests replacement of grains by authigenic quartz in the form of microcrystalline chert.

Barite occurs not only as euhedral crystals dispersed in the matrix and pores, but also in association with dissolution vugs typically containing calcite (Figure 9). Barite also displays irregular forms related to dissolution of foraminifera shells or other microfossils. Apatite often contains small quartz and pyrite inclusions. The porosity in this microfacies is typically associated with organic-matter pores, and pores within dissolution vugs and between mineral grains (Figure 8B).

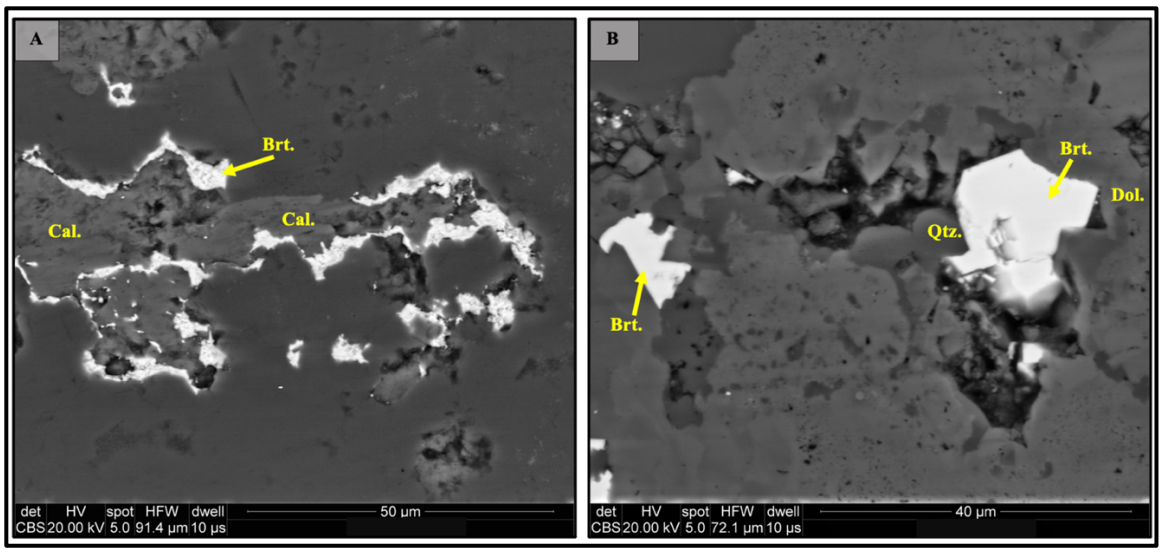

Figure 9. Backscatter SEM images. **A)** White material identified as barite (Brt.) based on energy dispersive analysis. Barite appears to be filling calcite (Cal.) dissolution vugs. **B)** Barite occurring in the matrix and as a late mineral phase filling pore spaces between dolomite (Dol.) and quartz (Qtz.) grains.

Sycamore Siltstone Microfacies

The calcitic siltstone microfacies (Figure 10A-B) are moderate to poorly sorted and consist of sub-angular to sub-rounded, medium to coarse quartz-silt (~35%), allochems (~20%), potassium feldspar (~15%), clay (~10%), ferroan dolomite (~8%), pyrite (framboidal and cubic), and minor sparse muscovite. The majority of the allochems occurs as non-skeletal grains such as peloids and calcispheres, and small amounts of skeletal grains including brachiopods. The carbonate peloids are largely composed of micrite whereas the calcispheres contain walls consisting of micrite or composed of larger single calcite crystals. The Alizarin Red S colors the majority of the allochems deep pink to red while the cement in the matrix does not stain for calcite (Figure 10B). Therefore, a combination of silica and clay cements exceeds the amount of calcite cement in the calcitic siltstone microfacies. Relict feldspars and dissolved feldspars which create pore spaces between grains are very common (Figure 11A-B). Thus, the typical pore types observed are secondary intragranular pores in dissolved feldspars (Figure 11C-D), and intergranular pores between framework grains (Figure 12A) such as dolomite and quartz. Minor porosity is also found in pyrite

framboids (Figure 12B) and in between clays, most commonly kaolinite [$Al_2Si_2O_5(OH)_4$] sheets (Figure 13).

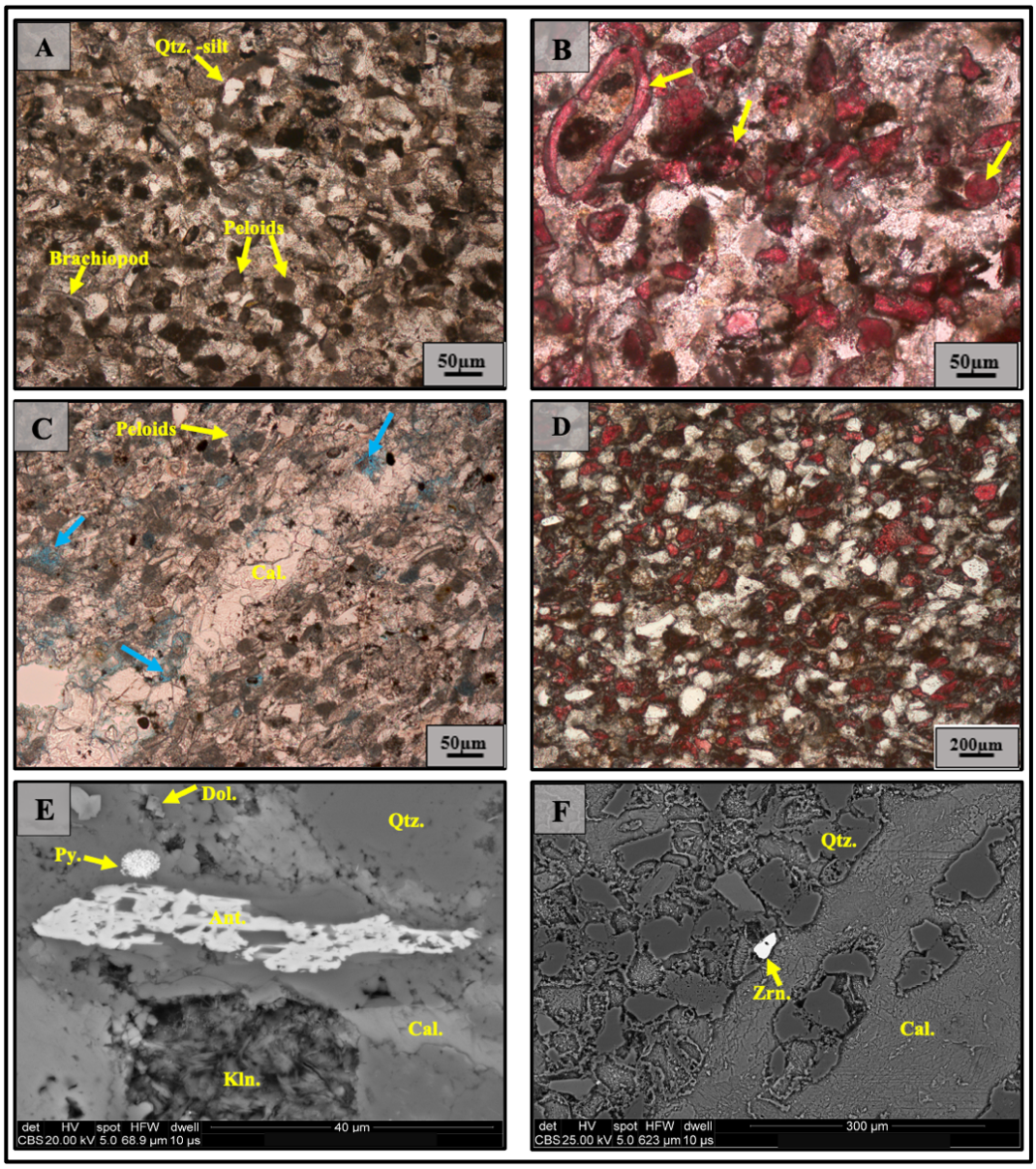

Figure 10. Representative microfacies of Sycamore siltstones. Plane Polarized Light (PPL) photomicrographs in A, B, C, and D. Backscatter SEM images in E and F. **A)** Calcitic siltstone microfacies. **B)** Calcitic siltstone stained with alizarin red S (ARS). Yellow arrows denotate that allochems stained deep pink to red for calcite. Note that a pervasive calcite cement does not occur in this microfacies. **C)** Calcite-cemented siltstone with a vertical mineralized fracture. Blue arrows demonstrate intergranular pore spaces. **D)** Calcite cemented siltstone stained red for calcite indicating a pervasive calcite cement. **E)** Major mineral phases in calcitic siltstone microfacies including framboidal pyrite (Py.), anatese (Ant.), dolomite (Dol.), and kaolinite (Kln). **F)** Calcite cemented microfacies with a vertical calcite vein, zircon (Zrn.), and quartz (Qtz.) grains.

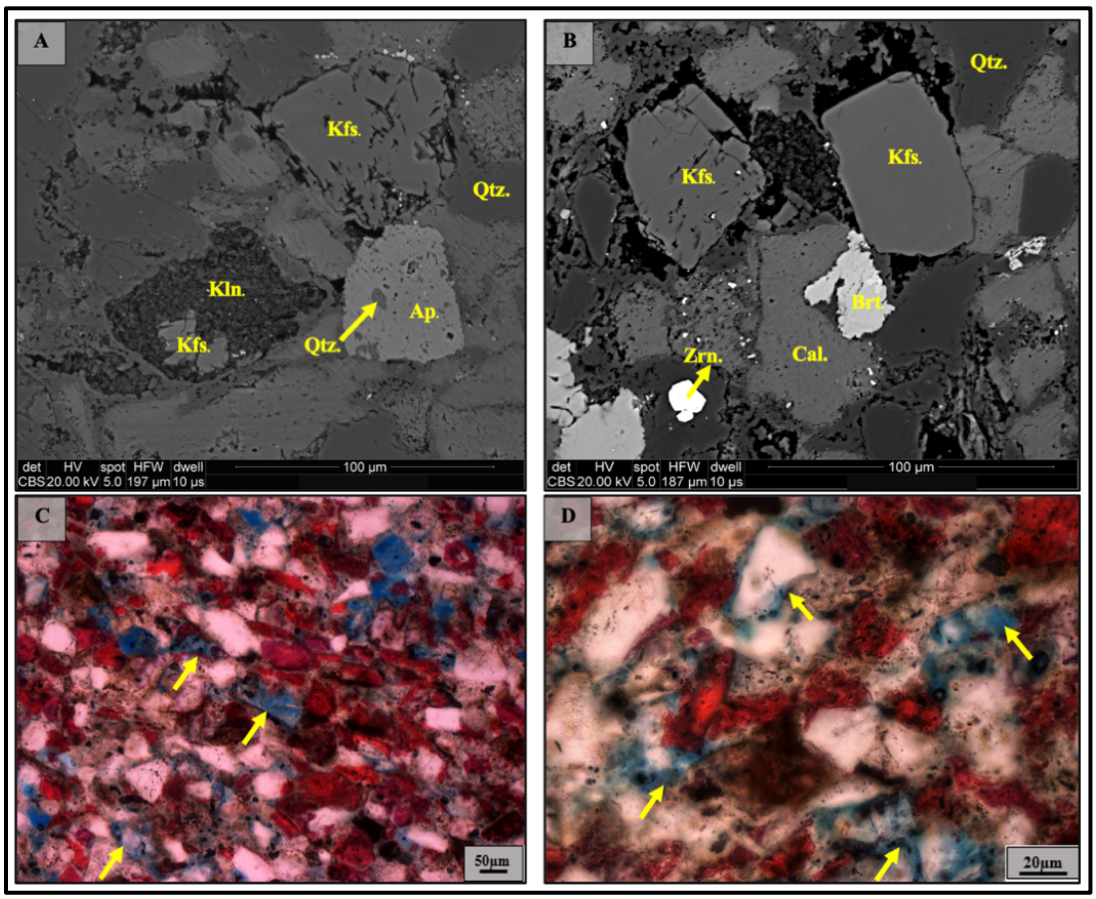

Figure 11. Secondary porosity as a result of dissolution of potassium feldspar (Kfs.) within Sycamore rocks. Backscatter SEM images in A and B. Plane polarized light (PPL) and stained photomicrographs in C and D, while blue color represents the porosity of the rock. **A)** Partially dissolved feldspar (Kfs.) in the top right. Kaolonite (Kln.) replacement of feldspar in the lower left. Apatite (Ap.) with quartz (Qtz.) inclusions in the lower right. **B)** Partially dissolved feldspars (Kfs.) creating secondary porosity. Other typical mineral phases in calcitic siltstones include zircon (Zrn.) and barite (Brt.). **C)** Yellow arrows indicate dissolved feldspar grains resulting in dissolution porosity. **D)** Yellow arrows denotating intergranular porosity between quartz grains and dissolution porosity.

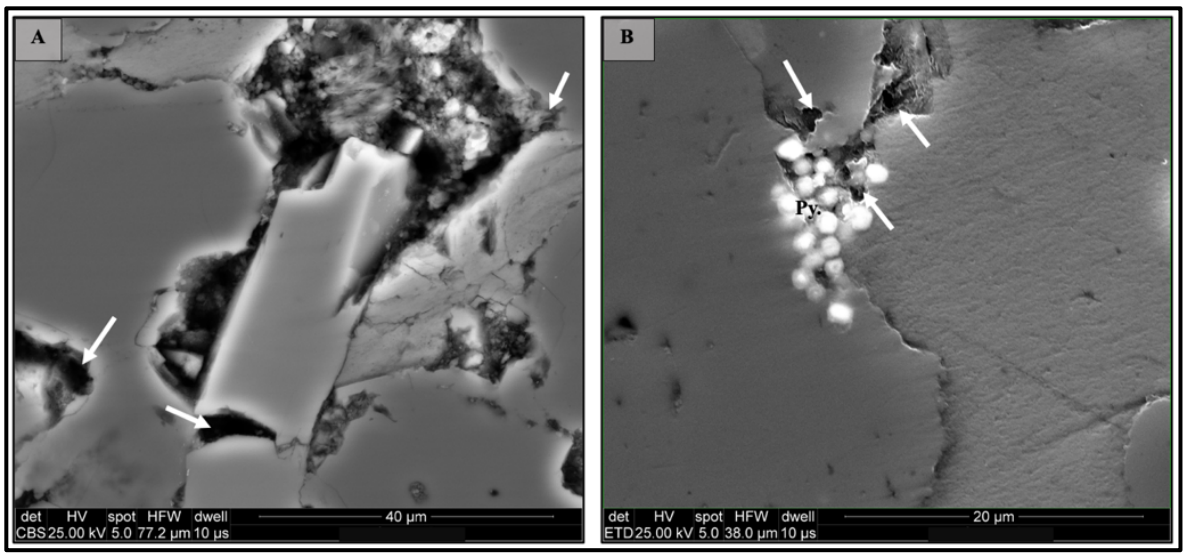

Figure 12. Common pore-types in Sycamore siltstones. Backscatter SEM images. White arrows are denotating the pore spaces. **A)** Intergranular pore spaces. **B)** Porosity associated with pyrite framboids.

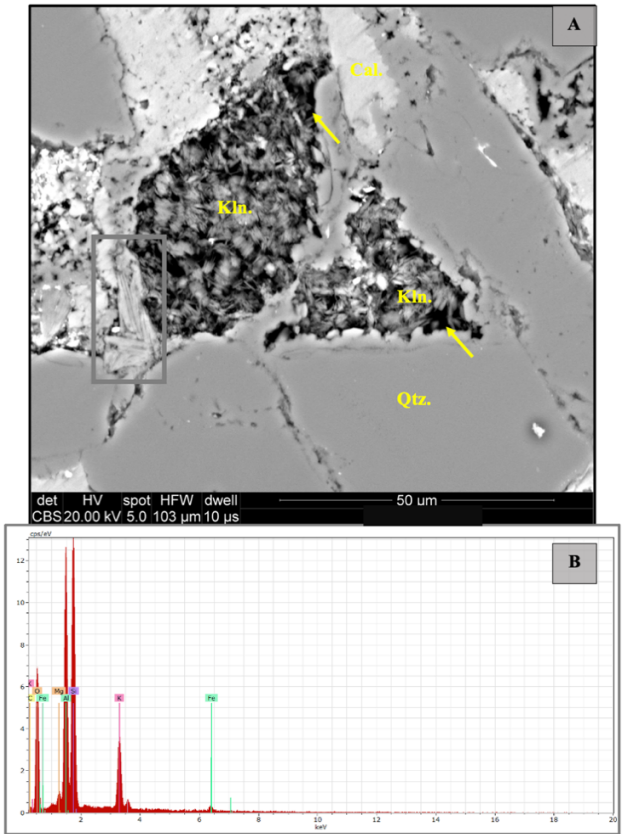

Figure 13. Common types of phyllosilicates in Sycamore siltstones. Backscatter SEM image in A and energy dispersive analysis graph in B. **A)** Two common types of clays in Sycamore rocks- Kaolinite (Kln.) and illite (gray box). The yellow arrows indicate pore space associated with clay structure. **B)** Graph showing the elemental composition of a point in the illite grain within the gray square. Illite is the stable potassium-rich 2:1 clay with concentrations of aluminum (Al), silicon (Si), and oxygen (O).

Dolomite crystals appear in the calcitic siltstone microfacies as euhedral rhombs, filling fractures, replacing other phases, and as cement (Figure 14A-D). SEM elemental composition mapping shows zoned dolomite crystals, evidence of alteration due to evolving fluids (Figure 15). Some detrital quartz grains are replaced by dolomite as well. Additional detrital grains present in the matrix include zircon ($ZrSiO_4$) (Figure 10F). Moreover, authigenic phases such as barite ($BaSO_4$), anatase (TiO_2), and halite (NaCl) are sparsely distributed in the matrix. Stylolites were only observed within mineralized fractures which have been subjected to brecciation and some degree of deformation.

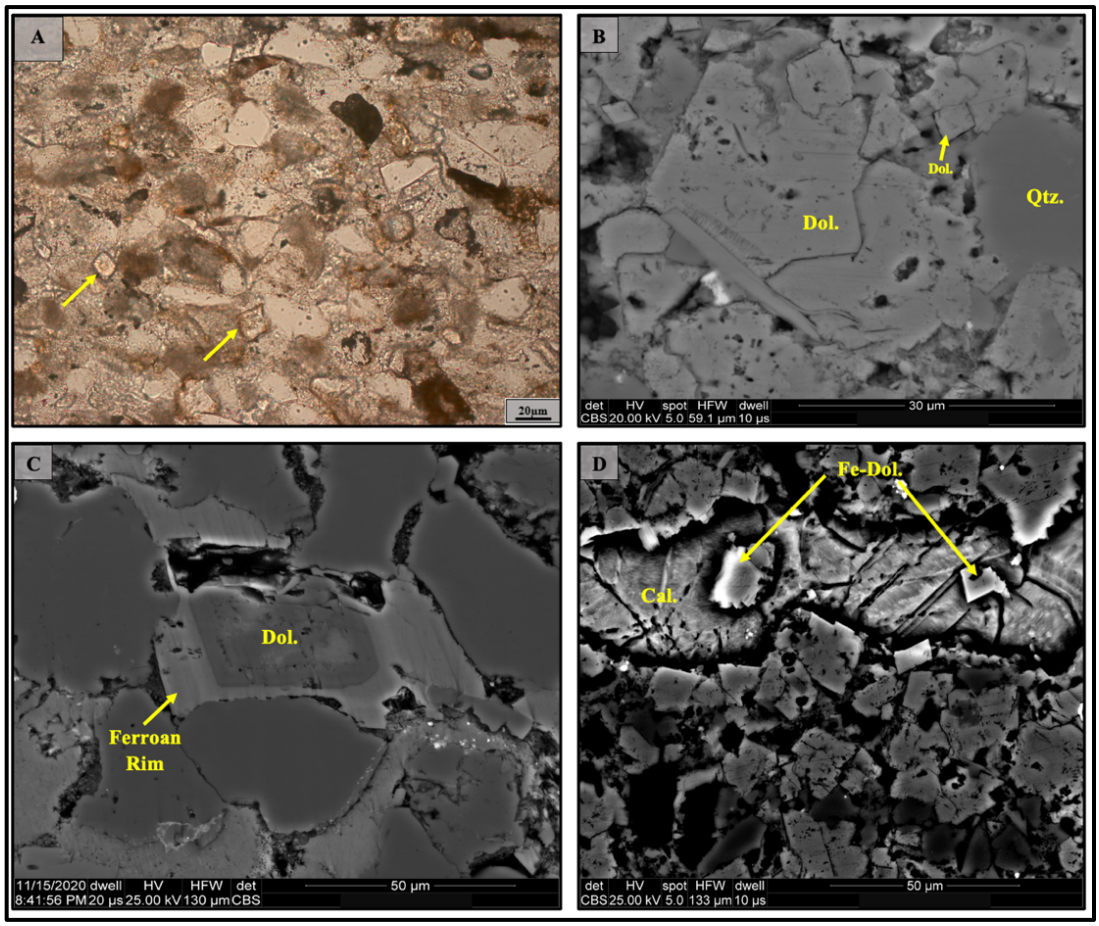

Figure 14. Occurrence of dolomite (Dol.) and ferroan dolomite (Fe-Dol.) in Sycamore siltstones. Plane polarized light (PPL) microphotograph in A. Backscatter SEM images in B, C, and D. **A)** Yellow arrows pointing to euhedral dolomite rhombs distributed in the matrix. **B)** Dolomite grains within a mineralized vein. **C)** Dolomite zoned by authigenic ferroan dolomite rim. **D)** Ferroan dolomite within a calcite-filled fracture.

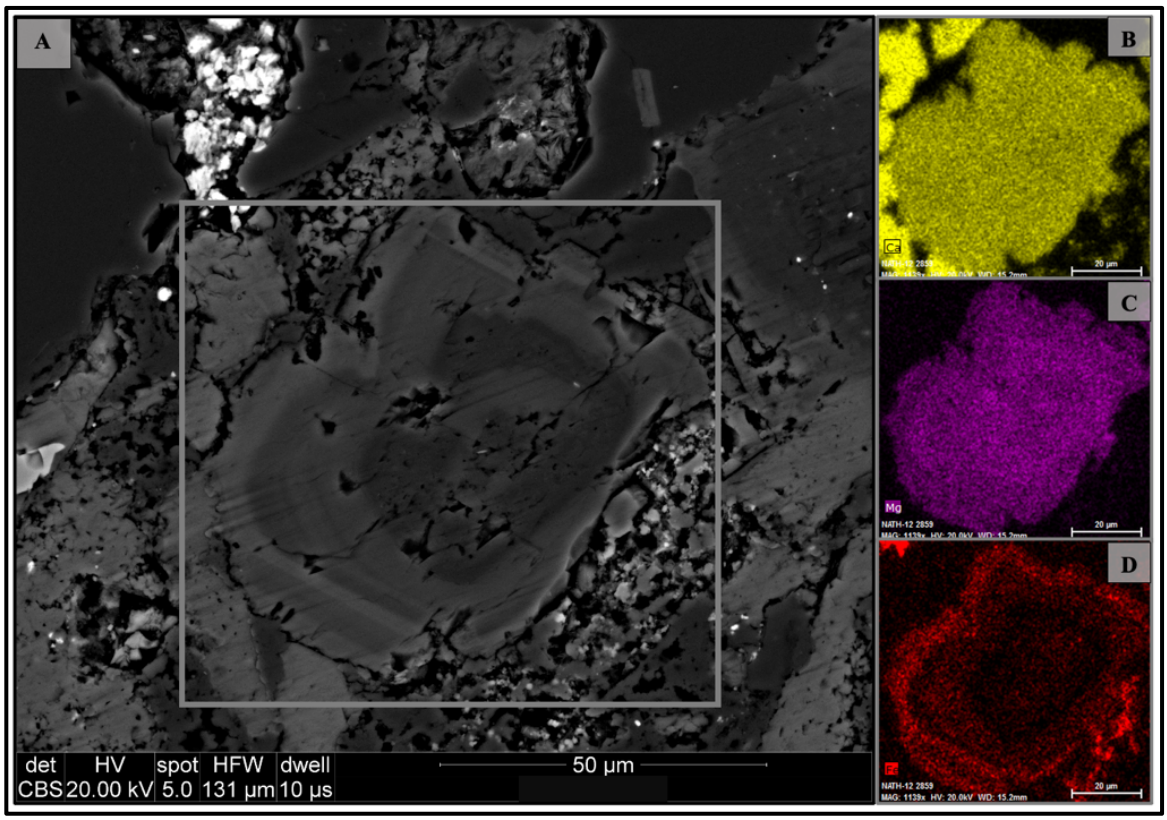

Figure 15. A clast of dolomite zoned by an authigenic ferroan dolomite rim. Backscatter SEM image in A. Elemental mapping in B, C, and D. **A)** Fe-dolomite within the gray square. Note the gradational changes in color and sharp contacts suggesting changes in composition between dolomitizing fluids during evolving stages. **B)** Elemental mapping of the Fe-dolomite grain indicating the presence of calcium (Ca). **C)** Elemental mapping of the Fe-dolomite grain indicating the presence of magnesium (Mg). **D)** Elemental mapping of the Fe-dolomite grain indicating the presence of an iron-bearing rim (Fe).

The calcite-cemented siltstone microfacies (Figure 10C-D) contains nearly the same mineral composition and diagenetic features as the calcitic siltstone microfacies except that the former contains pervasive calcite cement (Figure 10D) and less dissolved feldspar grains. In some zones, the calcite-cemented microfacies appear to exhibit a loosely packed "floating grain" texture without point-to-point grain contacts (Figures 16 A-C). Although large calcite crystals are dominant, calcite cement also occurs in lesser proportions as micrite possibly grading into finer-grained calcite anhedral crystals (Figure 16D**)**. Locally, most of the calcite cement occurs as

medium to large crystals filling intergranular pore space, fractures, and secondary dissolution features in unstable grains such as potassium feldspars.

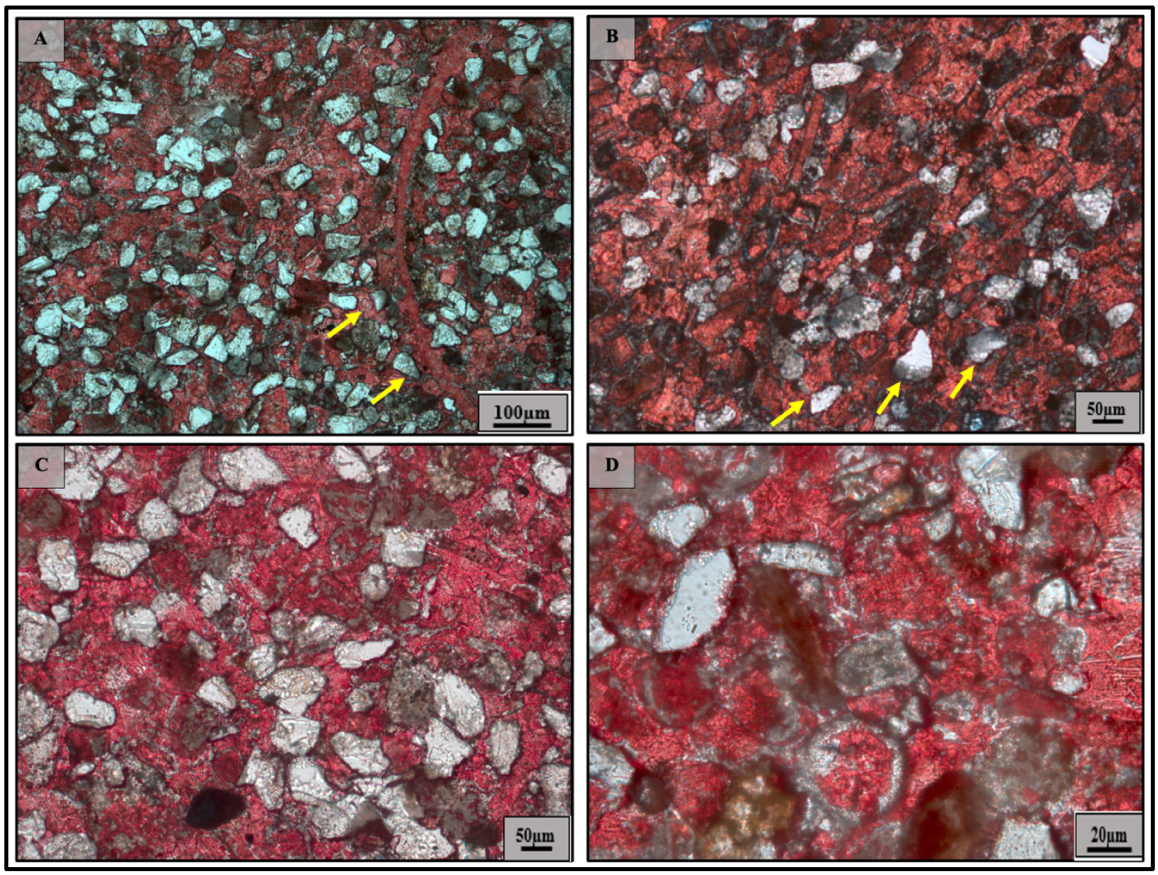

Figure 16. Calcite cemented siltstone microfacies. Plane polarized light (PPL) microphotographs stained red for calcite. Some quartz-silt grains in **A**, **B**, and **C** appear to be floating (yellow arrows) suggesting a syn-depositional calcite cementation. **D)** Some calcite seems to be dissolving as well as possible calcite grains grading into micrite through the process of neomorphism.

The mosaic of blocky calcite cement crystals hosts a series of authigenic and detrital phases including pyrite, zircon, and quartz grains. In addition to the pervasive calcite cement, calcite is also present in peloids (Figure 10C) and in small to medium-sized (between 20 to 50 µm) skeletal allochems including bryozoan and echinoderms. The calcite-cemented microfacies in the North Flank, specifically in the Middle Sycamore Section (MSyS), contain a large volume of silica precipitating before the calcite cement with evidence of dissolution before the silica precipitation.

The silica tends to precipitate in the outer rims of the calcite grains creating very accentuated and distinctive compositional zones between grains (Figure 17). Authigenic carbonate-apatite grains are found in the matrix (Figure 18).

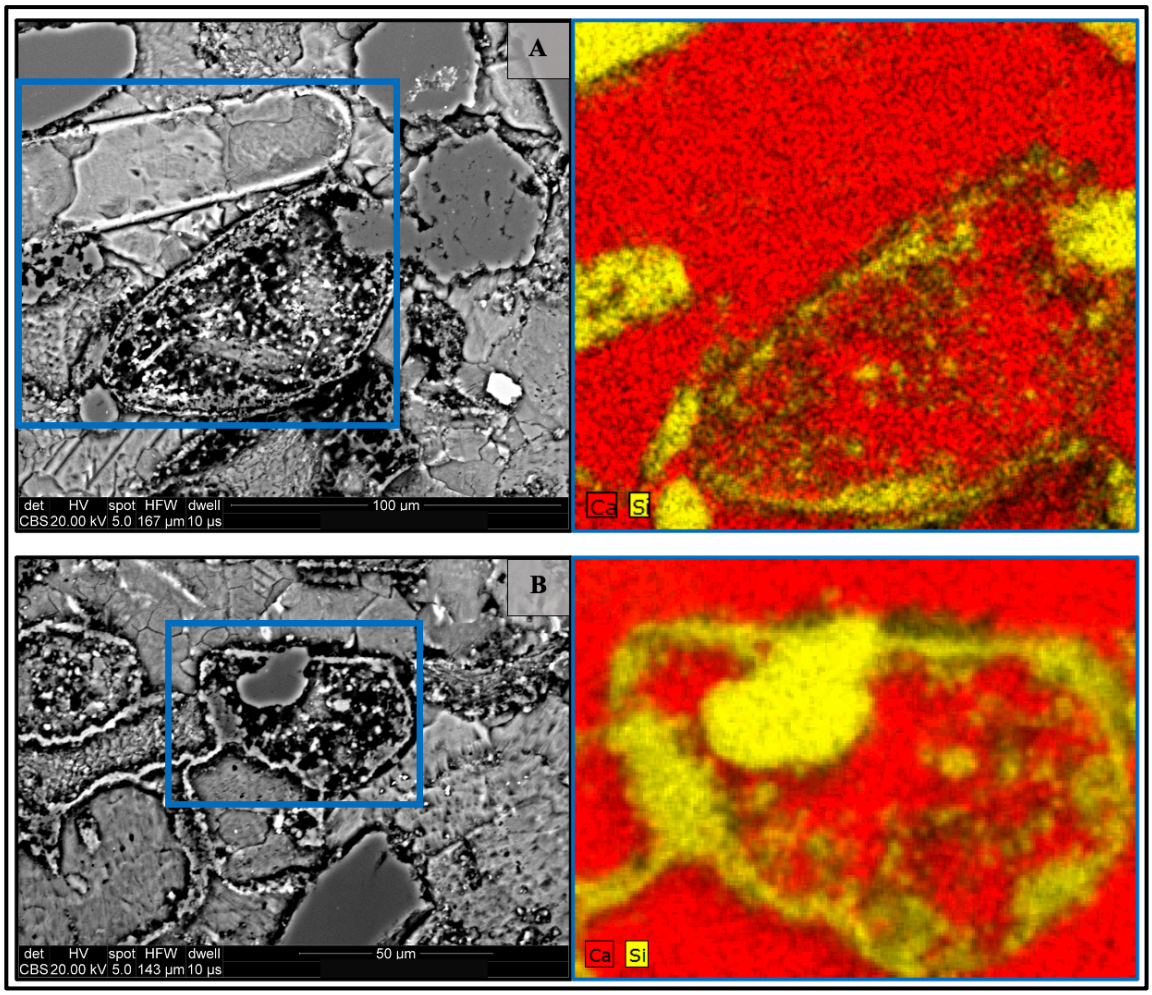

Figure 17. Variation of calcite cemented microfacies in the northern flank of the Arbuckle Anticline. **A) and B)** show precipitation of silica in outer rims of calcite grains, a phenomenon that is not common in calcite cemented microfacies from the southern flank. Elemental mapping (right) shows evident compositional boundaries between calcium (Ca) and silicon (Si).

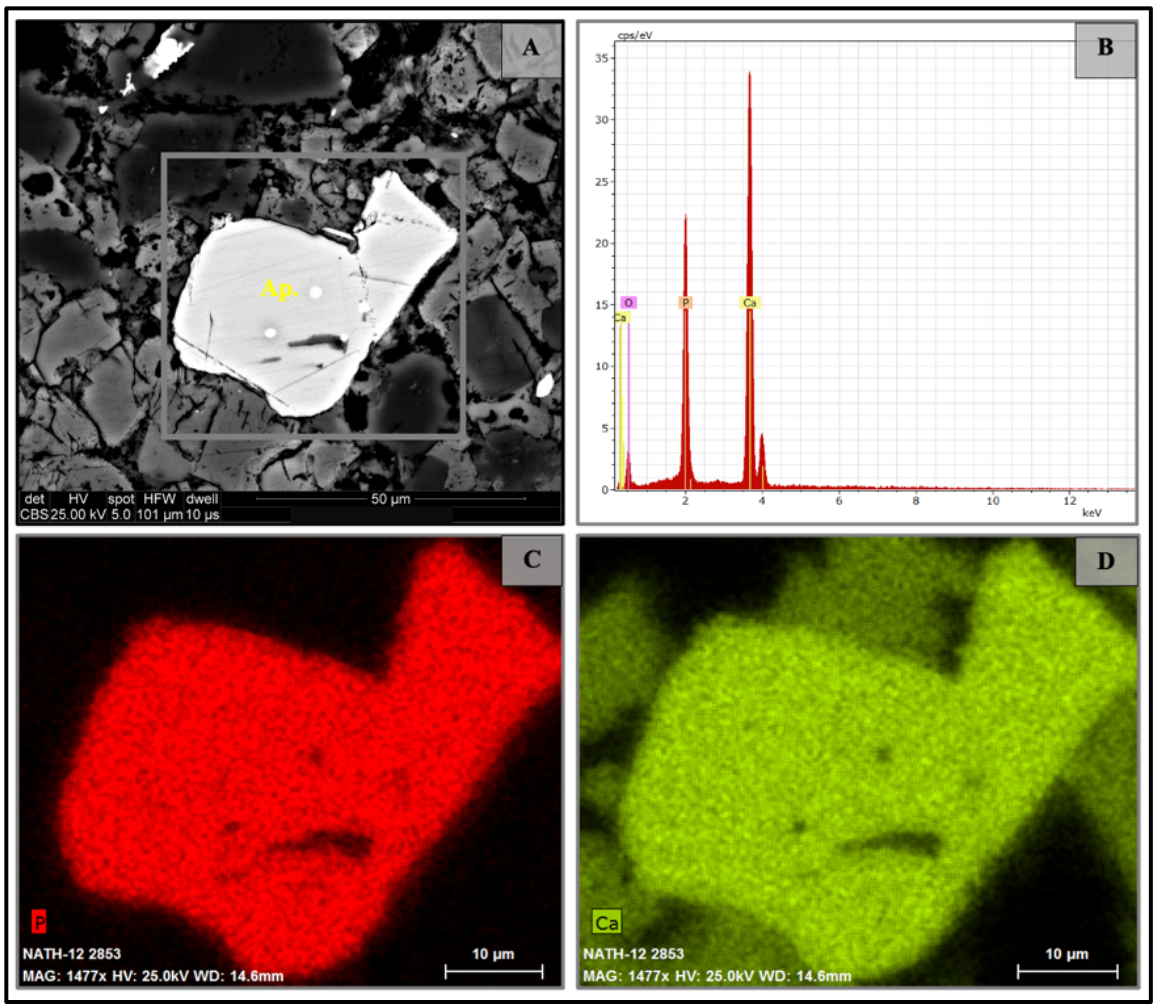

Figure 18. Apatite (Ap.) crystal present in the matrix of Sycamore rocks. Backscatter SEM image in A, energy dispersive analysis graph in B, elemental mapping in C and D. **A)** Euhedral apatite crystal inside the gray square. **B)** Energy dispersive analysis graph illustrating the major chemical elements constituting the apatite crystal in the gray box. These being phosphorous (P), calcium (Ca), and oxygen (O). **C)** Elemental mapping of the apatite crystal showing abundant phosphorous composition. **D)** Elemental mapping of the apatite crystal showing abundant calcium composition.

Fractures present in the siliceous mudrock microfacies (Figure 19A) and in the siltstone microfacies (Figures 10C and 19B-D) are complex with multiple cross-cutting fracture patterns. The fractures are dominantly vertical to sub-vertical in nature, some with evidence of fracture-related brecciation (Figures 19C and 20A). Fracture sets are primarily filled with large euhedral calcite and detrital quartz grains (Figure 19B-D). Small dolomite rhombs are observed along the boundaries of the fractures and less commonly, fractures are also filled with euhedral pyrite,

authigenic quartz, stylolites, and bitumen as isolated blobs or at triple junctions of grain boundaries (Figure 20B). The simple wave-like and suture-type stylolites cross-cut large idiomorphic calcite grains and fragments of the host rock present inside mineralized fractures (Figure 19B). These stylolitic seams are highlighted by a residue of insoluble opaque minerals (e.g., pyrite and/or hematite) or organic matter. Petrographic observation reveals that brecciation occurred right before stylotization based on textural relationships. Authigenic quartz occurs as a late fracture filling phase by permeating the open spaces available in vertical fractures between the carbonate phases. Quartz overgrowths are poorly developed, if any, they are not common in the samples analyzed. Later fractures exhibit sharper edges and are more predominant as we move stratigraphically up towards the Middle Sycamore Section (MSyS).

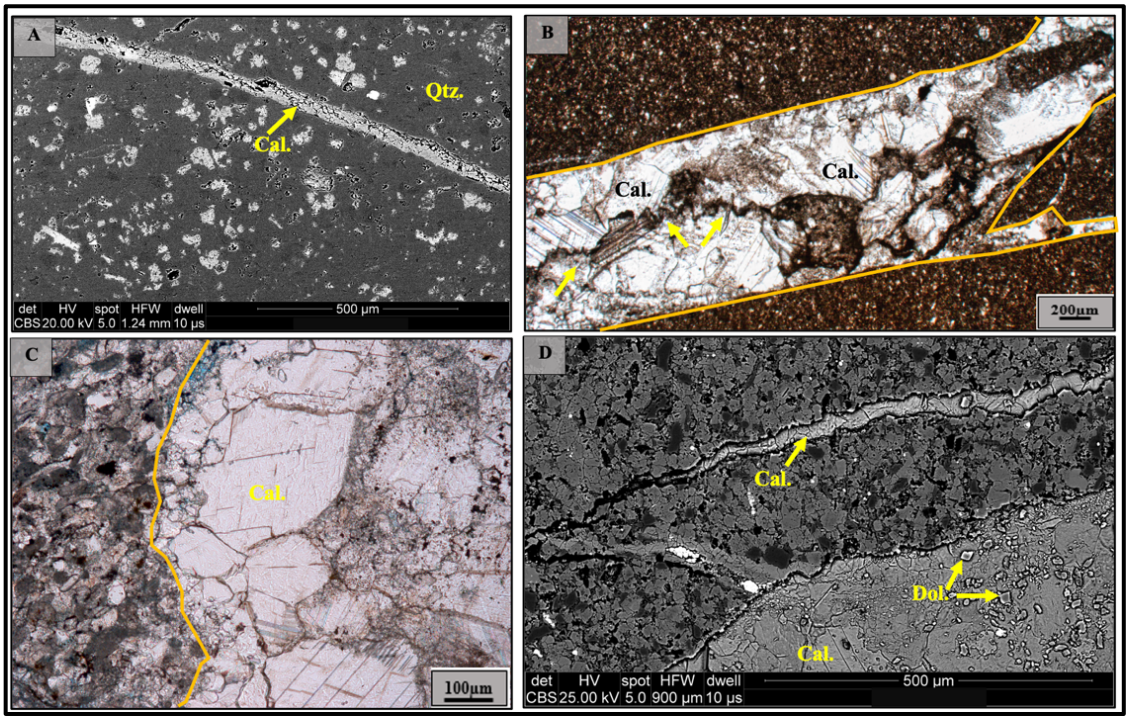

Figure 19. Vertical fractures and fracture-fill in the Sycamore Formation. Backscatter SEM images in A and D. Plane polarized light (PPL) microphotographs in B and C. **A)** Calcite-filled fracture in siliceous mudrock. **B)** Vertical fracture filled with calcite (Cal.), quartz grains, and fragments of the host rock. Stylolites (yellow arrows) cut through the fracture. **C)** Vertical fracture filled with large euhedral to subhedral calcite (Cal.) grains with evidence of brecciation in the lower right corner. **D)** Two vertical fractures filled with calcite and minor dolomite rhombs indicated by yellow arrows.

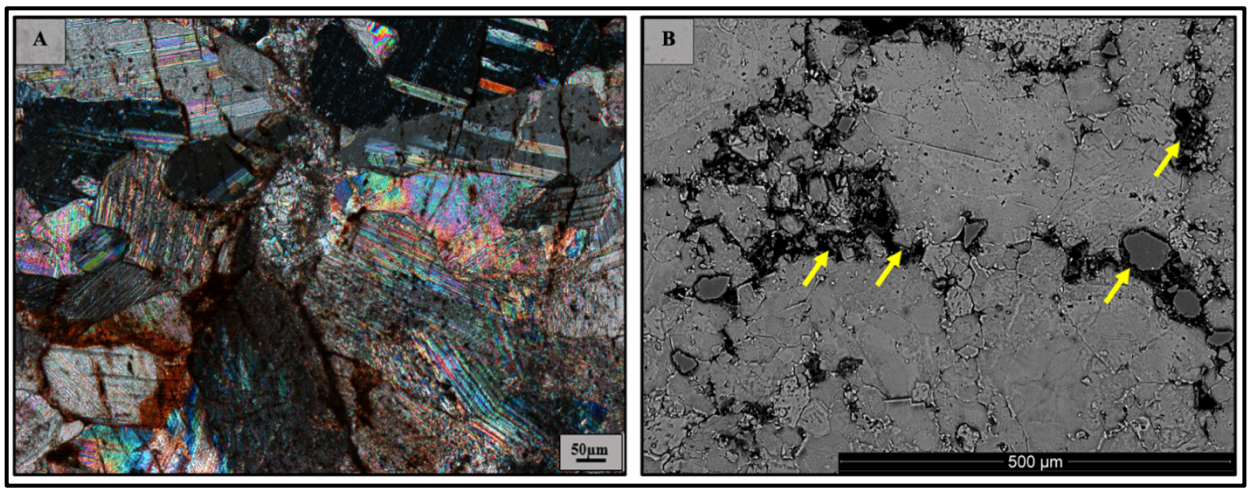

Figure 20. Cross polarized light (XPL) in A. Backscatter SEM image in B. **A)** Brecciation within calcite-filled fractures. **B)** Yellow arrows indicate hydrocarbon within calcite-filled fractures. Based on energy dispersive analysis, the dark material contains significant carbon composition.

5.2. Paragenetic Sequences

Since the occurrence of diagenetic events in the Sycamore Shale member differs from the ones observed in the Sycamore Siltstone ("Limestone") member, the parageneses of the Sycamore Formation was divided into two distinctive sequences. One sequence outlines the major diagenetic events observed in the Sycamore Mudrock ("Shale") member which includes the argillaceous, calcareous, and siliceous mudrock microfacies (Figure 21). The other sequence depicts the diagenetic events observed in both the calcitic siltstone and calcite-cemented facies representing the Sycamore Siltstone ("Limestone") member (Figure 22). The diagenetic stages presented in each sequence are subdivided into early, middle, and late stages. Early diagenesis refers to processes that occur near to the sediment surface that may be influenced by seawater at lower pressures and temperatures or perhaps by meteoric fluids if the sediment was exposed to it. Conversely, late diagenesis consists of processes occurring at depth, elevated temperatures (conventionally at temperatures lower than 300°C), and beyond surface water influence (Bjørlykke, 1998). For the most part, early to middle diagenesis in the Sycamore Formation is

dominated by events in the matrix and allochems, while middle to late diagenetic events are associated with fracturing and brecciation. The parageneses and diagenesis of the Sycamore formation are described in the next sections.

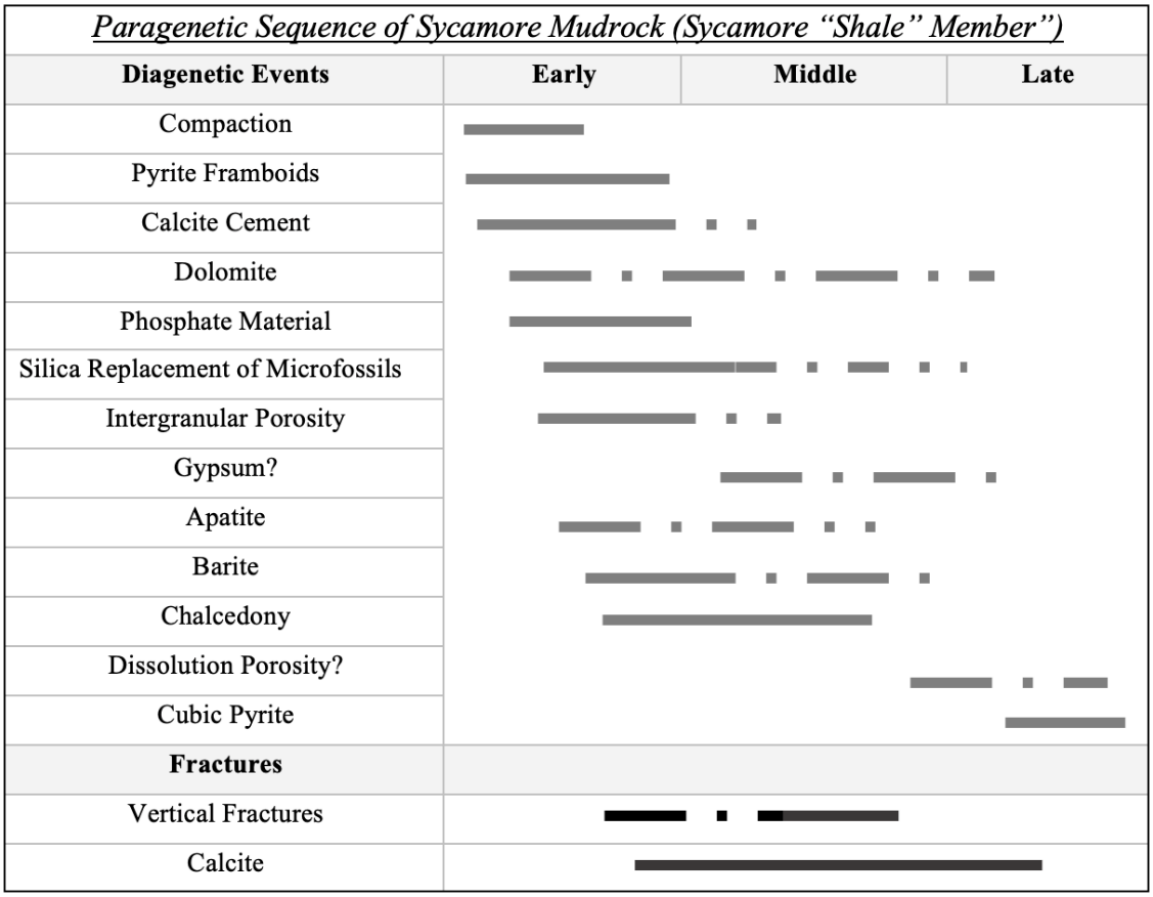

Figure 21. Paragenetic sequence for the Sycamore Mudrock, also known as the Sycamore "Shale" Member. The diagenetic events are listed from early to late, and the timing of the events is based on cross-cutting and textural relationships. Diagenetic events are divided into the ones occurring in the matrix and allochems versus the ones occurring within the mineralized fractures. Dashed line refers to uncertainty in timing of events.

Figure 22. Paragenetic sequence for the Sycamore Siltstone (Sycamore "Limestone" Member). The diagenetic events are listed from early to late, and the timing of the events is based on cross-cutting and textural relationships. Diagenetic events are divided into the ones occurring in the matrix and allochems versus the ones occurring within the mineralized fractures. Dashed line refers to uncertainty in timing of events.

5.3. Diagenesis of Sycamore Mudrock ("Shale") Member

Framboidal pyrite is interpreted to represent the earliest diagenetic event (Figure 21) within the near surface environment, and its occurrence is interpreted to have formed as a result of seawater sulfate reduction as indicated by Schieber (2011). The presence of distorted fabrics visible on a microscope scale such as deformed muscovite flakes and flattened microorganisms suggests that compaction resulted in these fabrics at earlier diagenetic stages (e.g., Prothero and Schwab, 2013). The intergranular calcite cement in the calcareous mudrock facies was precipitated during early diagenesis because it is next to the detrital grains. Perhaps the precipitation of intergranular calcite cement occurred in the absence of quartz cement, and if clay coats were common, it would be reasonable to imply that the clay coats would have prevented the nucleation of quartz overgrowths as well (e.g., Pittman et. al., 1992). The intergranular calcite cement might have been derived from internal sources in the system including dissolution of calcium-bearing allochems and feldspars (e.g., Morad et al., 1990; Moore, 2001). Alteration of clays in the interbedded mudrocks might have also provided the essential ions to precipitate carbonate cements (e.g., Sun et al., 2019).

Dolomite rhombs occur mostly as a secondary phase replacing the precursor mineral calcite during early to middle diagenesis, though some dolomite could also appear as a late mineral phase within mineralized fractures. The phosphate grains are detrital and interpreted to be sourced from collophane that precipitated from seawater. Similarly, both apatite and barite may have formed from seawater and then been remobilized and precipitated during early diagenesis. Various barite crystals might have only precipitated after the development of dissolution porosity due to the fact that irregular forms of barite fill dissolution pores.

The cryptocrystalline form of silica, chalcedony, contributed to the silicification of allochems during early to middle diagenesis based on its occurrence in skeletal debris. The overall silica replacement of microfossils is interpreted to be early to middle diagenesis as proposed in other studies which attribute silica replacement of fossils as a result of simultaneous dissolution of fossils and precipitation of authigenic silica at shallow burial depths (e.g., Schieber et al., 2000; Milliken and Olson, 2017). The silica present in the Sycamore mudrock facies is interpreted to be mostly derived from alteration of siliceous microfossils such as radiolarians during early diagenesis (e.g., Schieber et al., 2000; Milliken and Olson, 2017). Chalcedony might have precipitated from opaline silica which might have been released from the dissolution of siliceous microorganisms at near surface conditions (Prothero and Schwab, 2013).

The formation of pores in Sycamore mudrocks is interpreted as a relatively continuous process. The intergranular pore development is interpreted to be an early to middle diagenetic event as described in other studies (e.g., Er et. al., 2016, Wang et.al., 2016) while dissolution pores between grains probably occurred during later diagenesis. Compaction at an early diagenetic stage triggered the reduction of pore volume as fine-grained materials were compacted and clay floccules were compressed. With increasing chemical compaction and burial depth, the dehydration and conversion of clay minerals might have caused the development of the intergranular and/or intercrystalline pores between authigenic clays during early to middle diagenesis (Zhang et. al., 2019). Based on cross-cutting relationships, authigenic cubic pyrite marks the late stages of diagenesis with some evidence of fine crystalline pyrite occluding intergranular pores. The low abundance of mineralized fractures in the Sycamore “Shale” supports previous studies which have reported that burial of Sycamore “Shale” has resulted in minor amounts of fracturing (e.g., Terrell, 2019).

5.4. Diagenesis of Sycamore Siltstone ("Limestone") Member

Diagenesis within the Sycamore Siltstone "Limestone" Member was marked by near surface cement precipitation followed by compaction and fracturing (Figure 22). The early marine calcite cement is the primary authigenic phase variably occurring in each Sycamore siltstone microfacies, and surrounding silt-sized grains, skeletal fragments, and peloids. For the calcitic siltstone facies, the high clay volume may have resulted in the low concentrations of calcite cement. The authigenic silica which locally occurs in the matrix may also have contributed to the low amount of calcite cement. In some instances, the siltstone microfacies contain partially dissolved allochems which could be the primary source of calcite cement if the grains were dissolved during the diagenetic evolution of the sediment (e.g., Al-Ramadan et. al., 2005). Due to seawater typically being saturated with calcium carbonate, calcite cement could have been derived directly from saturated seawater or from partial dissolution and reprecipitation of carbonate grains specifically skeletal allochems which can provide nucleation surface for calcite cementation (Brenner et. al., 2010; Morad, 2010).

The occurrence of calcite cemented silt grains with a floating texture (Figures 16A-C), in the absence of quartz cement, implies that the calcite cement was syn-sedimentary in origin (e.g., Ulmer-Scholle et al., 2015; Xiong et. al., 2016). Hence, in this particular setting, the cementation process occurred soon after deposition and prior to the earliest stages of mechanical compaction. The fact that micrite could possibly grade into the coarser calcite suggests that the latter replaced the micrite during neomorphism (Figure 16D). The process of neomorphism could account for the development of the aforementioned "floating" texture in the Sycamore siltstone microfacies. It is also possible that the calcite formed soon after deposition since Mississippian seas represent a transitional period between calcite-dominated seas to aragonite and high-magnesium calcite seas

(Ries, 2010). The composition of the calcite cement is likely the low-magnesium end-member of calcite since high-Mg is relatively unstable past surface conditions (e.g., Molenaar, 1990; Prothero and Schwab, 2013). If calcite cement was indeed syn-sedimentary, it formed before compaction and contributed to the "floating texture" by preventing the grains from being in close contact to each other.

The precipitation of framboidal pyrite is interpreted to represent an early diagenetic stage based on its isolated occurrence in the matrix and previous interpretations that associate it with sulfate reduction (e.g., Folk, 2005; Schieber, 2011). The occasional pyrite laminae in some specimens probably indicates it was concentrated in organic-rich zones (e.g., Berner et al., 1985). Dolomite occurring in the matrix and as a replacement of allochems is interpreted as forming during early to middle diagenesis, whereas the dolomite in fractures precipitated during middle to late diagenesis. Ferroan dolomite is interpreted as forming during early to middle diagenesis when iron and magnesium were available in the system as a result of clay conversion or local dewatering of shales. Changes in dolomite grains from a non-ferroan core to a ferroan rim with sharp transitional contacts probably indicates stages in which dolomitizing fluids entered the system (Figure 15).

Quartz cement is not abundant in the siltstone microfacies nor are quartz overgrowths. The small amount of quartz cement in the Sycamore siltstone microfacies might be related to a combination of factors including possible unfavorable burial temperatures (below 60°C or above 80°C), and large volumes of early calcite cement (e.g., Bjorlykke and Egeberg, 1993; Rahman and Worden, 2016; Walderhaug, 2000). Experimental work on the solubility of silica conducted by Blatt (1982) reveals that quartz nucleates and precipitates so slowly that deep burial and longtime spans are required. Though a significant amount of quartz cement can only be produced at great

depths, minor quartz cement can still be produced through other various mechanisms. Assuming that pressure solution from mechanical compaction was minor in the Sycamore Formation, the small amount of quartz cement may have been primarily derived from biogenic silica (e.g., Milliken and Olson, 2017; Schieber et. al., 2000) which is common in the Sycamore mudrock microfacies. Alternatively, quartz may be formed from silica released during the conversion of smectite-to-illite in the course of early to middle diagenesis (e.g., Sivalingam, 1990; Thyberg et. al., 2010). Another possible source of the minor quartz cement could have been from alteration of feldspars and micas subsequently releasing silica into the system (e.g., Bjørlykke, 1988; Sun et al., 2019).

The dissolution of feldspars (Figure 11) is identified as burial in origin, and it is the principal mechanism for the presence of secondary porosity in the Sycamore Formation. Previous studies suggest (e.g., Worden and Barclay, 2000; Yuan et. al, 2015) that dissolution of feldspars occurs in the presence of CO_2 along with acidic and organic-rich fluids. These fluids could be sourced from the internal clay-rich mudrocks within the Sycamore Formation, or more likely from the underlying organic-rich Woodford Shale. Due to the organic richness of the Woodford Shale (Miceli Romero and Philp, 2012; Cardott, 2012), it is reasonable to infer that the CO_2 released during decarboxylation of organic matter in aqueous solution contributed to the development of acidic fluids that caused the dissolution of feldspars in the Sycamore Formation. The conversion from smectite to illite could have also be one of the potential mechanisms for the source of the dissolving fluids (e.g., Ulmer-Scholle et al., 2015).

The magnitude of feldspar dissolution is more pronounced in the calcitic siltstone microfacies. Perhaps the pervasive calcite cement in the calcite cemented siltstone reduced the permeability of the rock; and thus, creating impermeable zones affecting how acidic fluids

interacted with unstable feldspar grains and ultimately leading to less dissolution of these grains. The dissolved feldspar grains also supply ions to precipitate illite which is one of the most common authigenic clays in the Sycamore Formation. Although most of the illite is interpreted to have formed from smectite conversion during early to middle diagenesis, some illite is also interpreted to be coeval with the pores within dissolved feldspars during middle to late diagenesis. Since some dissolution pores and related clay minerals contain bitumen linings, it suggests that illitization and hydrocarbon migration might have occurred around the same time during paragenesis. However, maturation of hydrocarbons probably occurred during the smectite-to-illite conversion in early stages of diagenesis (Pevear, 1999).

The carbonate-apatite (Figure 18) found in the matrix of the siltstone microfacies may have precipitated from seawater or formed due to dissolution and reprecipitation of phosphatic material during early diagenesis (e.g., Nesse, 2017). Barite occurs isolated from other phases and determining the relative timing is difficult. It can precipitate from seawater sulfate during hydrothermal activity (e.g., Hanor, 2000) or form during early diagenesis as a result of remobilized barium and sulfate material. It is crucial to point out that hydrothermal alteration associated with both barite and apatite has been documented in the Woodford Shale in Southeastern Anadarko Basin, Oklahoma (Roberts et al., 2019). Therefore, it is possible that the barite could be hydrothermal in origin. Titanium oxides, likely anatase, are interpreted as occurring during middle diagenesis based on textural criteria.

Mineralized fractures (Figure 19) crosscut the other diagenetic features such as the calcite cement which indicates that they formed after the calcite and probably during late diagenesis. As previously mentioned, the fractures are filled with calcite, dolomite, quartz/chalcedony, pyrite, and they also contain stylolites (Figure 19B). Authigenic silica in the mineralized fractures implies that

it precipitated during late diagenesis based on the textural criterion. Following near surface diagenesis, the Sycamore siltstone underwent burial and compaction which aided in the development of mineralized fractures and stylolites. The presence of hydrocarbons in intergranular pores in the matrix, in dissolved grains, and in the fractures suggests that the hydrocarbon migration occurred after dissolution events during late diagenesis.

5.5. Paleomagnetism

Thermal demagnetization of the Sycamore Formation in the southern flank reveals a south-southeasterly component (Figures 23A-B). The component is a characteristic remanent magnetization (ChRM) unblocked at relatively high temperatures ranging from 100 °C to 450 °C with a south-southeasterly declination and relative shallow inclinations (~17°). A poorly defined steep component is also removed in some specimens at low temperatures ranging from 100 °C to 175 °C (Figures 23C-D) and is interpreted as a viscous remanent magnetization (VRM). While exposing the specimens to an alternating magnetic field (AF demagnetization), a similar ChRM was isolated from 10 mT to 100 mT with southeasterly declination and moderate up inclination (Figure 24). Demagnetization of northern flank specimens resulted in southeasterly directions, but the mean angles of deviation (MAD) are unacceptable (>18°) for calculation of mean statistics (Fisher, 1953). Alternating field demagnetization of the Woodford Shale samples produced a linear decay with southeasterly declinations and positive inclinations (Figure 25).

There is a general southeasterly grouping of the specimen directions for the southern flank Sycamore specimens (**Geo.**: Dec= 129°, Inc= 3.6°, k= 14.91, α95= 13.8°, n/n_o: 06/12; **Strat.**: Dec= 124.6°, Inc= 8.3°, k= 14.43, α95= 15.1°, n/n_o: 06/12; Figure 26), especially in the Lower and Middle Sycamore Sections of the southern flank. The ChRM in the Woodford Shale had a better

grouping (**Geo.**: Dec= 135.1°, Inc= 3.7°, k= 74.08, α95= 5.6°, n/n_o: 07/07; **Strat.**: Dec= 136.8°, Inc= -8.7°, k= 152.57, α95= 3.9°, n/n_o: 07/07; Figure 26) than the specimens in the Sycamore Formation. Performing a fold test was not possible due to the poor data quality from the north flank Sycamore specimens. Based on the CRM mean geographic directions, the pole position for the Sycamore Formation in the south flank has a latitude of 30.2°N and longitude of 147°E (dp= 6.9; dm= 13.8; Figure 27), and the pole position for the Woodford Shale has a latitude of 20.1°N and longitude of 127.5°E (dp= 3.9; dm= 6.6; Figure 27). The pole position for the mean stratigraphic directions in the Sycamore Formation have a latitude of 25.3°N and longitude of 148.2°E (dp= 7.7; dm= 15.2; Figure 27), whereas the Woodford Shale has a latitude of 40.1°N and longitude of 146.2°E (dp= 2; dm= 3.9; Figure 27).

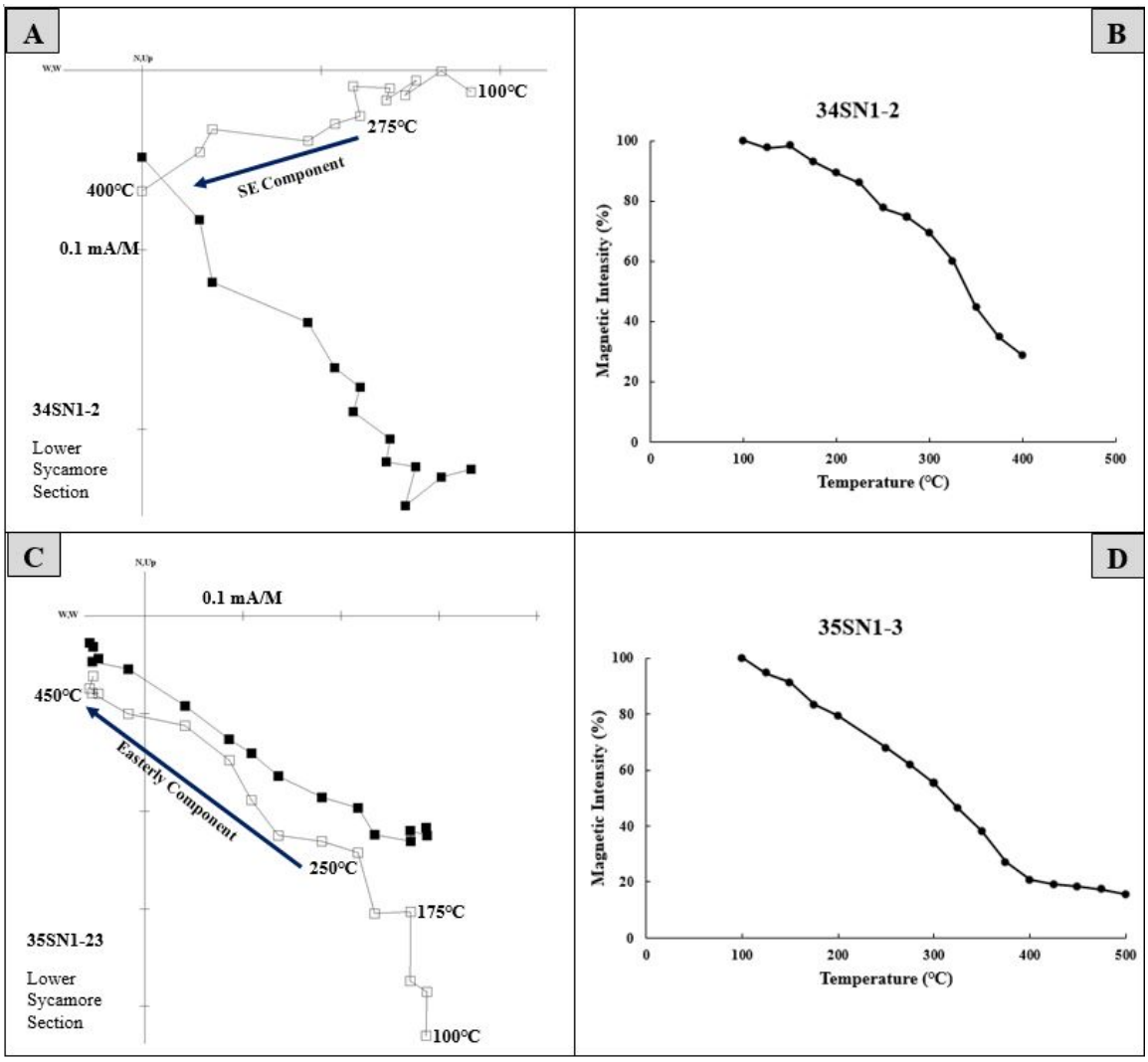

Figure 23. Representative Zijderveld diagrams for thermal demagnetization in the Sycamore Formation, southern flank of the Arbuckle Anticline, I-35 Outcrop **(A and C)**. Closed squares represent the horizontal component of the magnetic field whereas open squares represent the vertical component. The NRM was removed from both figures because of high intensity and to better illustrate the thermal decay. Both specimens are from the Lower Sycamore Section. **A)** The unblocking temperature of the ChRM is from 275 °C to 400° C. The magnetic component has a Declination= 135.6°; Inclination= -11.1°; and MAD angle= 8.7°. **C)** The unblocking temperature of the ChRM is from 250°C to 450°C. The magnetic component has a Declination= 121.3°; Inclination= 29.9°; and MAD= 5.6°. **B and D)** Magnetic intensities versus temperature plots of each respective specimen.

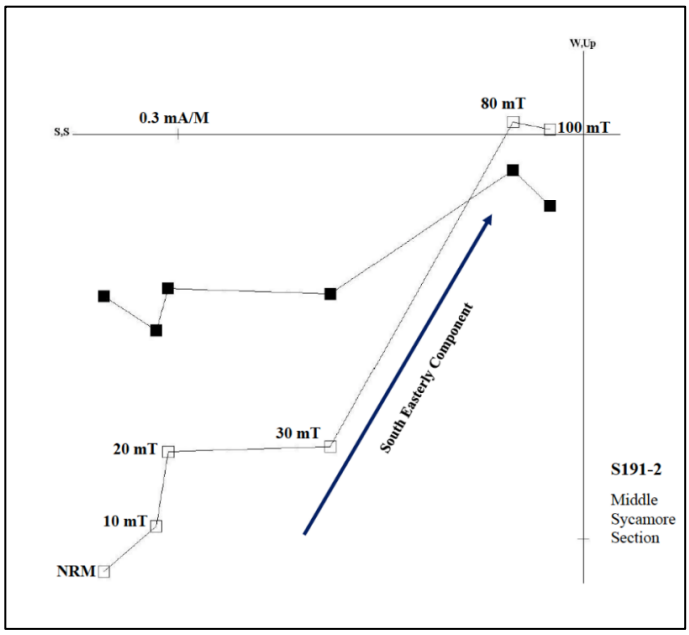

Figure 24. Representative Zijderveld diagram for AF demagnetization in the Sycamore Formation, southern flank of the Arbuckle Anticline, I-35 Outcrop. Closed squares represent the horizontal component of the magnetic field whereas open squares represent the vertical component. The ChRM was isolated from 10mT to 80mT. Magnetic component has a Declination= 160.5°; Inclination= 44.8°, and MAD= 9.8°.

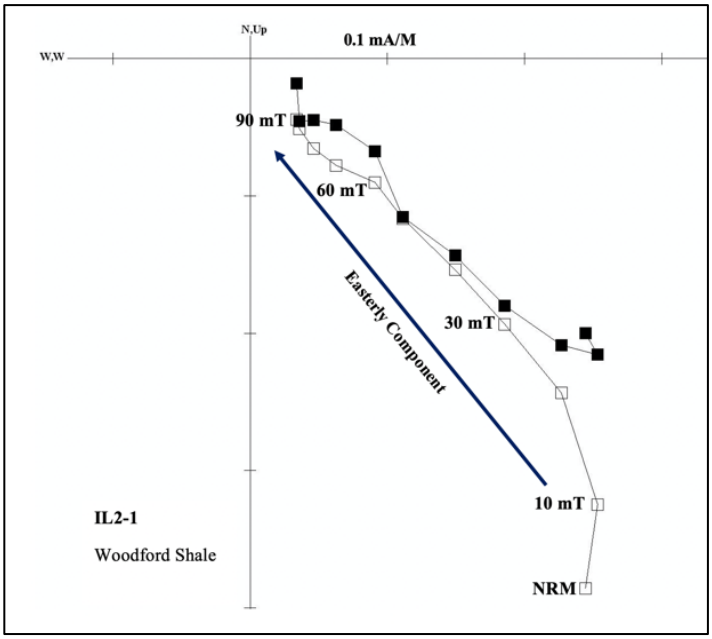

Figure 25. Representative Zijderveld diagram for alternating field demagnetization in the Woodford Shale, southern flank of the Arbuckle Anticline, I-35 Outcrop. Closed squares represent the horizontal component of the magnetic field whereas open squares represent the vertical component. The unblocking temperature of the ChRM is from 10 mT to 90 mT. The magnetic component has a Declination= 131.5°; Inclination= 40.9°; and MAD angle= 7.6°.

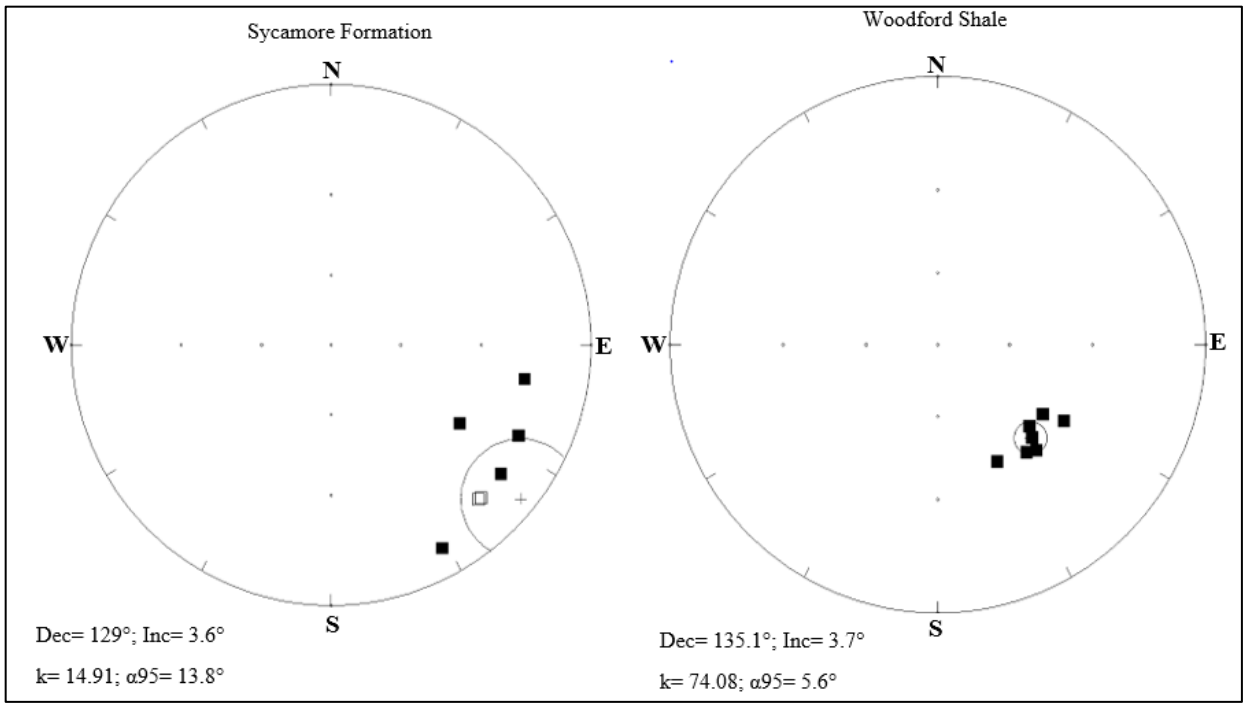

Figure 26. Equal-area plots of the ChRM specimen directions of the Sycamore Formation (left) and Woodford Shale (right). Declination values are measured clockwise from north. Inclination is measured from 0° at the edge of the circle and 90° at the center of the circle. The closed squares represent directions in the lower hemisphere with down inclinations whereas the open squares represent directions in the upper hemisphere with up inclinations. The smaller circles and the plus symbol represent the α95 confidence limit and the mean direction, respectively.

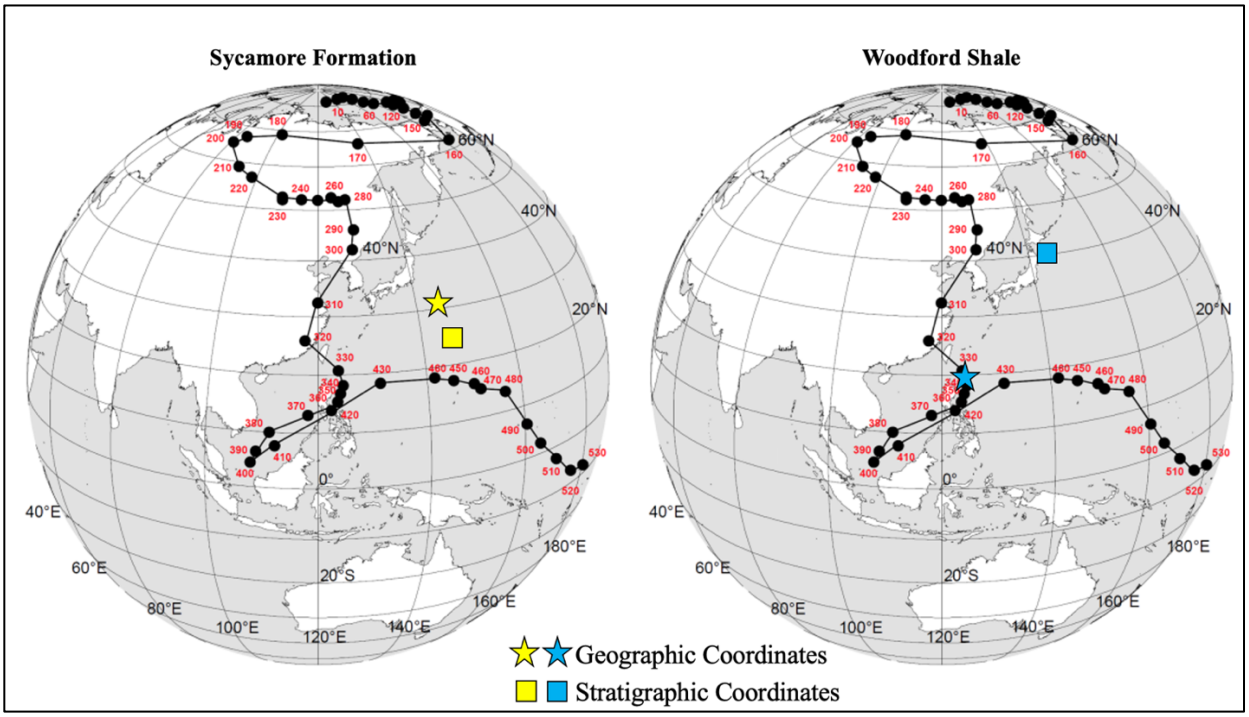

Figure 27. Apparent Polar Wander Path (APWP) for North America. The calculated virtual geomagnetic pole (VGP) for the CRM is depicted by the yellow color for the Sycamore Formation (left) and the blue color for the Woodford Shale (right). The star represents mean geographic coordinates while the square represents mean stratigraphic coordinates. The VGP latitude and longitude were calculated from the declination and inclination values from the specimens as well as the latitude and longitude of the study area. The pole position plots off the APWP for the Sycamore Formation, but it plots between Late Devonian to Early Mississippian for the Woodford Shale in geographic coordinates. Conversely, the pole position plots off the APWP for both the Sycamore Formation and the Woodford Shale in stratigraphic coordinates. Modified from (Torsvik et. al., 2012).

5.6. Anisotropy of Magnetic Susceptibility

Magnetic susceptibility values from the studied specimens range from a minimum of 1.789 x 10^{-5} SI to a maximum of 2.37 x 10^{-4} SI, although for most of the specimens (roughly 95%), mean susceptibility (k_m) values range between 2.0 and 7.0 10^{-5} SI. The AMS results display significant diversification between sites. The sites are subdivided into three groups based on the AMS results. One group consists of two sites which have steep K1 axes (Sites 7 and 9; Figure 27) perpendicular to the bedding plane. A second group contains only one site (Site 3; Figure 28) in which K1 has a shallow inclination in stratigraphic coordinates. The third group consists of most sites without a

great deal of consistency. Representative AMS results for these variable sites are shown in figures 29 (Site 8) and 30 (Sites 2 and 6). The presence of prolate to triaxial fabrics throughout the Sycamore Formation is interpreted to be carried mostly in paramagnetic minerals since the mean susceptibility values are positive (Table 3) (Tarling and Hrouda, 1993; García-Lasanta et. al., 2013).

Site	*N*	k_m (x 10^{-6})	σ (x 10^{-6})	*L*	σ (x 10^{-6})	*F*	σ (x 10^{-6})	*Pj*	σ (x 10^{-6})	*T*	σ (x 10^{-6})
S19- 9	9	65.80	11.31	1.010	0.002	1.008	0.001	1.019	0.003	-0.132	0.077
S19-3	11	66.35	7.318	1.011	0.001	1.002	0.001	1.014	0.002	-0.705	0.159
S19-5	10	31.32	3.262	1.012	0.010	1.017	0.017	1.030	0.027	0.083	0.277
S19-6	7	17.89	2.342	1.039	0.016	1.035	0.025	1.078	0.019	-0.088	0.483
S19-4	4	-	-	-	-	-	-	-	-	-	-
S19-8	9	70.48	15.72	1.009	0.004	1.005	0.003	1.014	0.004	-0.234	0.376
S19-1	-	-	-	-	-	-	-	-	-	-	-
S19-2	8	21.91	2.329	1.019	0.006	1.013	0.015	1.033	0.016	-0.304	0.394
S19-7	14	237.0	31.99	1.017	0.003	1.004	0.002	1.022	0.003	-0.598	0.193

Table 1. Summary of magnetic average scalar data for each site. *Site:* name of the site; *N:* number of specimens; k_m: mean susceptibility; *σ*: standard deviation; *L:* magnetic lineation; *F:* magnetic foliation; *Pj:* corrected anisotropy degree; *T:* shape parameter. Note that sites 1 and 4 were very challenging to drill for core samples resulting in unreasonable data for interpretation.

The uppermost (9) and lowermost (7) sites display a dominant linear prolate fabric with vertical to sub-vertical maximum axes that are perpendicular to the bedding plane, suggesting an inverse magnetic fabric (e.g., Rochette et al., 1992; Dudzisz et al., 2016). Site 7 has the highest k_m values amongst all the sites, and K3 and K2 tensors have a moderate girdle in directions in contrast to site 9 where K2 and K3 are shallow with NNW-SSE and WSW-NE directions (Figure 28). Specimens in site 3 have shallow inclinations with NNE-SSW declinations in stratigraphic coordinates. In the third group, some specimens from the Middle Sycamore Section (sites 1, 4, 5, 8) generally display scattering of the principal axis (e.g., Site 8; Figure 30) in geographic coordinates. Conversely, still in the third group, some sites exhibit well-grouped directions (e.g., Sites 2 and 6; Figure 31).

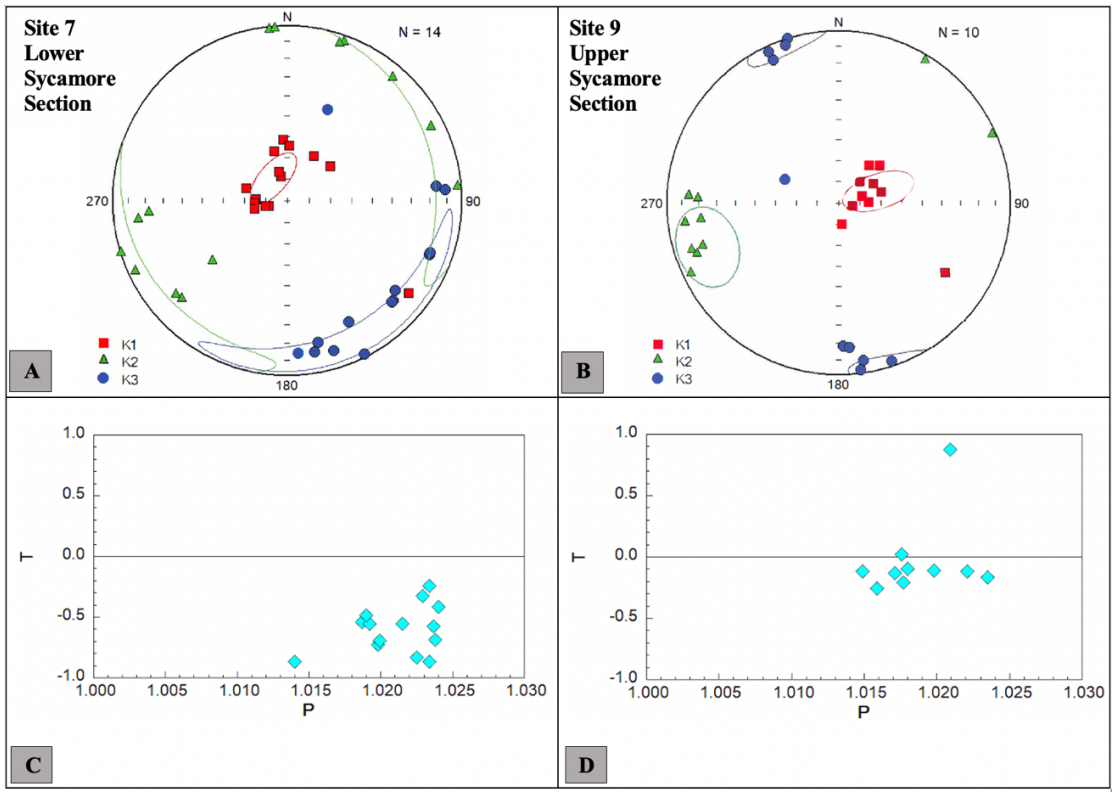

Figure 28. Representative data of the first group: **A)** and **B)** Equal area projections of AMS data from the lowermost (left) and the uppermost (right) sites of the Sycamore Formation in stratigraphic coordinates. K1 tensors are vertical to sub-vertical suggesting inverse AMS fabrics. Jelinek (1981) plots of the shape factor (T) versus degree of anisotropy (P) for **C)** site 7 and **D)** site 9. The diamond shape represents the specimens which indicate a prolate fabric. Each equal area plot displays confidence ellipsoids.

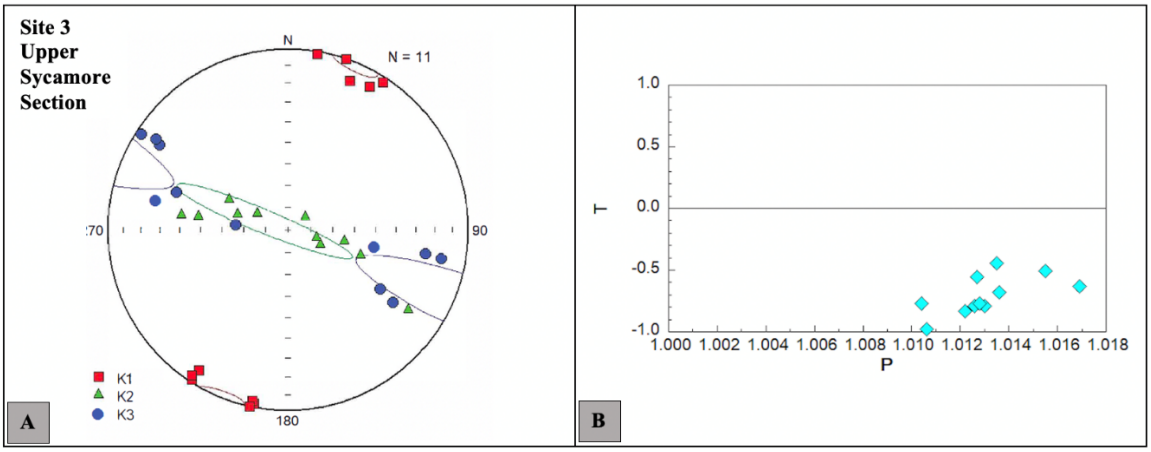

Figure 29. Representative data of the second group: **A)** Equal area projection with confidence ellipsoids from site 3 of the Sycamore Formation in stratigraphic coordinates. **B)** Jelinèk (1981) plot of the shape factor (T) versus degree of anisotropy (P) suggesting a prolate fabric.

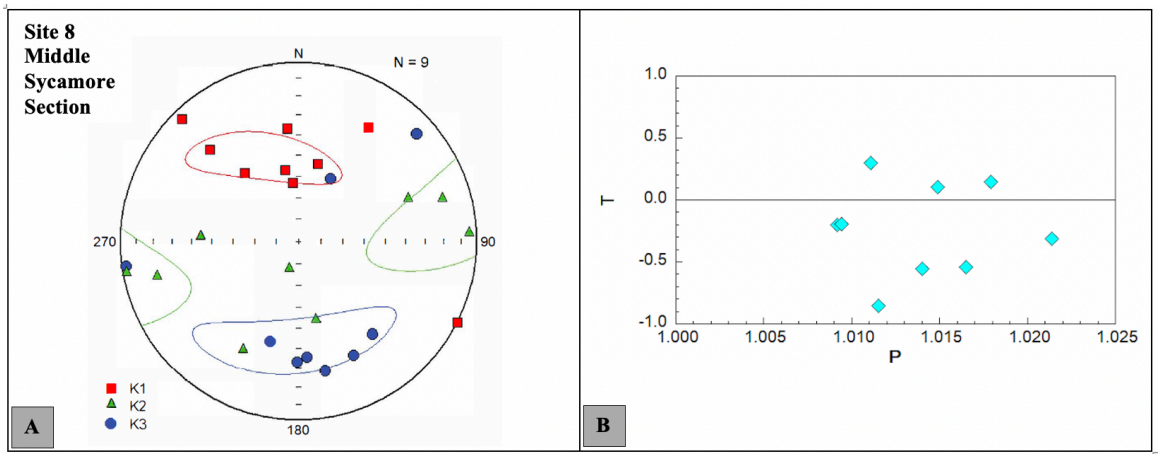

Figure 30. Representative data of the third group: **A)** Equal area projection with confidence ellipsoids from site 8 of the Sycamore Formation in geographic coordinates. The lack of consistent directions within principal axes and the complexities associated with composite magnetic fabrics makes it very difficult to interpret certain sites in the Sycamore Formation. **B)** Jelinèk (1981) plot of the shape factor (T) versus degree of anisotropy (P) suggesting a prolate

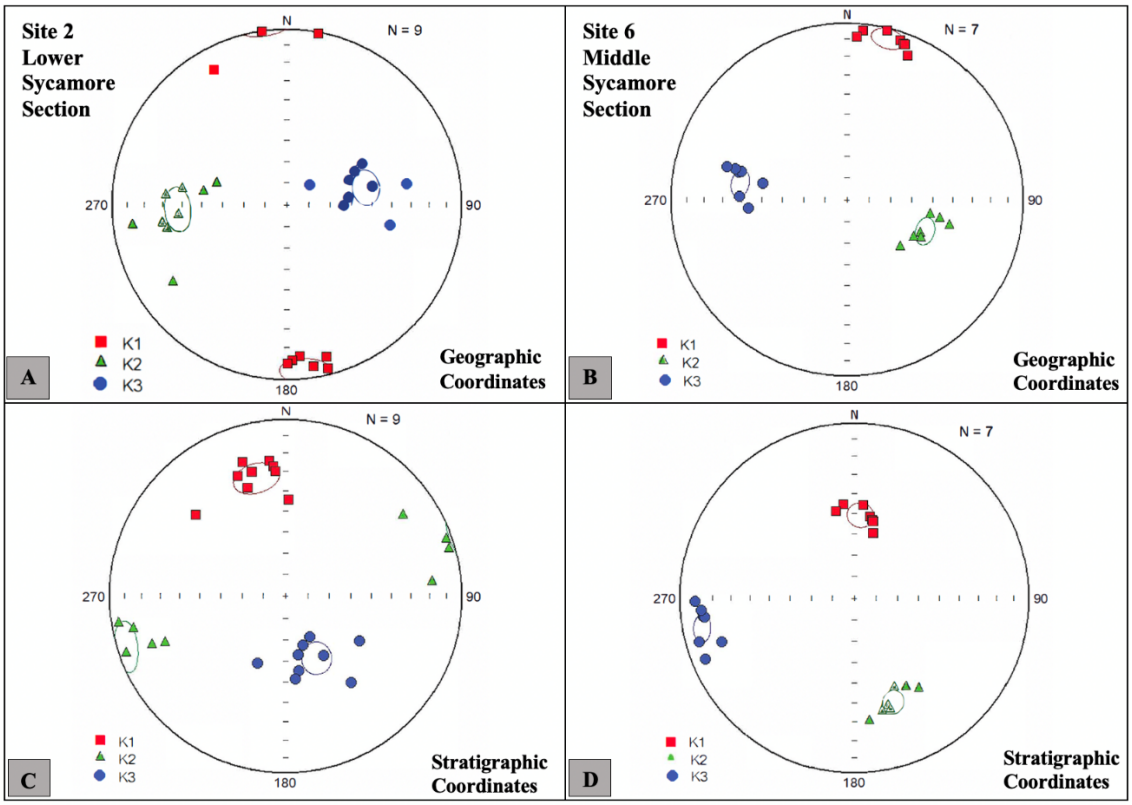

Figure 31. Representative data of the third group: **A)** and **B)** Equal area projections of AMS data from site 2 (left) and site 6 (right) of the Sycamore Formation in geographic coordinates. K1 appears nearly horizontal. **C)** and **D)** Equal area projections of AMS data from site 2 (left) and site 6 (right) of the Sycamore Formation in stratigraphic coordinates. K1 appears inclined after tilt correction. Each equal area plot displays confidence ellipsoids.

6. DISCUSSION

6.1. Controls on Diagenetic Alteration: Open vs. Closed System and Pore Development

The issue of whether the sequence of diagenetic events in a system is being controlled by lithology (closed system) or regional fluid migration (open system) remains a fundamental question in both siltstones and mudrocks (e.g., Roberts et al., 2019). Based on petrographic and SEM analysis, the diagenesis of the Sycamore Formation is interpreted to be primarily controlled by internal processes occurring during early diagenesis. In the course of middle to late diagenesis, the Sycamore Formation probably evolved into an open system as a result of external fluids causing dissolution of unstable grains and perhaps precipitation of ferroan dolomite.

During the formation of pyrite, silica replacement of microfossils, and calcite cement precipitation, the Sycamore Formation is interpreted to be largely closed to internal fluids. The calcite cement in the calcite cemented siltstone microfacies is interpreted to be syn-sedimentary or precipitated soon after deposition. Calcite cementation probably formed before compaction which resulted in the "floating texture." Since deposition of the Sycamore Formation occurred in the Mississippian during the transition from calcite to aragonite seas (Ries, 2010), then early calcite cementation is possible.

With increasing temperature and pressure during burial, a series of mineral reactions and phase changes likely released ions in aqueous solutions which became involved in diagenetic processes. After some burial, dewatering of the local interbedded mudrocks might have provided fluids for dissolution including those fluids that favored the precipitation of non-ferroan dolomite (Krajewski and WOŹN, 2009). Another process is the conversion of smectite to illite which can release a substantial amount of water which may have been a source of the dissolving fluids (e.g., Ulmer-Scholle et al., 2015). Illitization also releases cations such as Mg^{+2} and Si^{+4} which could

have contributed to the precipitation of dolomite and siliceous cements, respectively (e.g., Boles and Franks, 1979). One issue with the compaction model is that after mudrocks are compacted and dewatered, the expelled fluids tend to migrate vertically rather than laterally. In addition, mass balance equations reveal that compacting even an enormous volume of mudrock would result in dolomite equal to as little as 1% of the mudrock volume (e.g., Prothero and Schwab, 2013).

The zoned nature and chemical composition of the ferroan-dolomite observed in Sycamore siltstones suggests formation from evolving fluids characterized by variable content of magnesium, calcium, and iron (Figure 15). The origin of dolomitizing fluids is puzzling because dolomite is thermodynamically stable in seawater which is the most abundant Mg-bearing fluid. However, slow kinetics at near surface conditions tend to inhibit dolomitization while elevated temperatures as a result of burial or hydrothermal circulation tend to promote dolomitization (e.g., Zhang et. al., 2007). For Sycamore rocks, the origin of the dolomite is attributed to burial fluids (e.g., Blomme et. al., 2017).

As previously described, the dissolution of feldspars is interpreted as a being caused by burial fluids. In addition to illitization being one of the potential sources for the dissolving fluids, the generation of organic acids and CO_2 as a result of organic matter maturation in the underlying Woodford Shale and/or in the mudrock facies in the Sycamore could also be a source of such fluids (e.g., Ehrenberg and Jakobsen, 2001). Previous studies (e.g., Sassen et. al., 1987) propose that the onset of oil generation at vitrinite reflectance of about 0.55 % R_O produces organic fluids and CO_2. As a prolific source rock in Oklahoma, the average vitrinite reflectance value from the Woodford Shale in the I-35 outcrop is 0.50% R_O (Cardott and Chaplin, 1993). This suggests that these organic diagenetic processes occurring in the Woodford Shale and/or the Sycamore mudrock facies could

have led to the formation of subsurface fluids which triggered feldspar dissolution in the Sycamore Formation and produced secondary porosity.

Although the Woodford Shale is located in the same outcrop exposure as the Sycamore Formation, it is important to emphasize that composition of subsurface fluids can be due to the mixing of chemically unrelated waters and continuous rock-water interactions (Moore, 2001). Thus, it is likely that the diagenetic events in the Sycamore Formation were controlled by both internal and external processes. A series of internal fluids dominated the Sycamore during early diagenesis, but external fluids migrating from the Woodford Shale also contributed to development of the diagenetic events in Sycamore rocks. If the mudrock facies in the Sycamore Formation provided the organic acids, then the system could have been closed. It is not possible to determine the source of the fluids, although if the Woodford was involved, the Woodford-Sycamore interval may have behaved as a closed system.

Another mechanism that could cause alteration by external fluids would be through hydrothermal activity. Hydrothermal fluids are defined by convention as "aqueous solutions that are warm or hot relative to the surrounding environment" with temperatures 5°C–10°C higher than the host rock (White, 1957; Machel and Lonnee, 2002). Multiple hydrothermal minerals such as witherite, chalcopyrite, apatite, and among others have been observed in the Woodford Shale suggesting hydrothermal alteration during middle to late diagenesis in the Ardmore Basin (Roberts et al., 2019). Petrography and SEM observations in the Sycamore Formation do not show substantial evidence for hydrothermal activity. Some minerals which have been tied to hydrothermal alteration are observed, including barite and apatite (e.g., Bouzari et. al., 2016), but they are not strong evidence because they are not necessarily hydrothermal in origin.

6.2. Paleomagnetism

The ChRM identified in the Sycamore Formation is interpreted to reside in magnetite based on removal during AF demagnetization and unblocking temperatures below 580 °C. Removal of the component in the Woodford Shale by AF treatment also suggests that it resides in magnetite. The ChRMs identified in the Sycamore Formation and Woodford Shale are interpreted to be a chemical remanent magnetization (CRM) based on the low burial temperatures for the south flank samples. Vitrinite reflectance data from the Woodford Shale in the Arbuckle Mountains yields a weighted average of 0.54% R_O with estimated burial depth of 1.23 - 1.79 km and a maximum burial temperature of 56 – 70 °C (Cardott et al., 1990). Moreover, the average vitrinite reflectance value from the Woodford Shale in the I-35 outcrop is 0.50% R_O which also suggests burial temperatures less than 100 °C (Cardott and Chaplin, 1993).

Performing a fold test was not possible due to the poor data quality from the north flank specimens. The pole position for the Sycamore Formation is off the APWP for North America in both geographic and stratigraphic directions perhaps due to the poor grouping of specimens. Although the CRM is tentatively considered as post folding, defining the time of magnetization of Sycamore rocks is unattainable because a fold test could not be performed. Future work should focus on collecting samples from the Sycamore and the Woodford for a fold test.

The results suggest that the primary magnetization was destroyed and replaced by the secondary CRM which was acquired as a new magnetic mineral grew at low temperatures. Applying optical and SEM observations to identify ferromagnetic minerals can be arduous since these minerals are usually small (≤ 1μm for single domain or pseudo-single domain grains) and at very low concentrations (Butler, 1992). Both the ChRM in the Sycamore Formation (southern flank) and Woodford Shale (I-35 outcrop) display the same directions suggesting a similar

mechanism for the origin of the CRM. Possible remagnetization mechanisms include burial processes such as illitization reactions (e.g., Woods et al., 2002; Elmore et al., 2012), maturation of organic matter (Elmore et al., 2012) hydrocarbon migration (Elmore and Crawford, 1990), and orogenic fluids (Elmore, 2001; Elmore et al., 2012). Burial mechanism such as maturation of organic matter could be applied to the Woodford Shale since it is a source rock. However, a similar burial mechanism is less likely in the Sycamore siltstones because they are not a source rock and do not contain abundant illite. The Sycamore Formation does contain degraded hydrocarbons in pores; hence, hydrocarbon migration is possible (e.g., Elmore et al., 2012). Hardwick (2018) also identified a CRM held in magnetite in the Meramec Formation in the STACK play which is the equivalent of Sycamore rocks in southern Oklahoma. The CRM had poor grouping, but it was interpreted as acquired during a period of rapid subsidence associated with the Ouachita Orogeny (Hardwick, 2018).

To reiterate, the ChRMs identified in the Sycamore and Woodford Formations are interpreted to reside in magnetite and are chemical remanent magnetizations (CRMs) based on the low burial temperatures for the south flank samples. Unfortunately, no authigenic magnetite was found during the petrographic/SEM study, probably because it is present in low concentrations. The geographic and stratigraphic pole positions for the Sycamore Formation are off the APWP perhaps because of the poor grouping of specimen directions. Although the CRM is tentatively considered as post folding, defining the time of magnetization of Sycamore rocks is unattainable because a fold test could not be performed. The timing of the CRM in the Woodford Shale could not be constrained because a fold test was not possible.

6.3. Petrofabric

Magnetic anisotropy techniques have been commonly used to investigate paleocurrent directions (e.g., Schieber and Ellwood, 1993), examine patterns of strain in sedimentary rocks (e.g., Dudzisz et. al., 2016), and assess diagenetic alteration (Parés, 2015). Magnetic fabric in rocks can be acquired and developed through a series of multiplex processes dependent on the nature of the boundaries between grains, and both grain orientation and packing (Parés, 2015). The AMS ellipsoids from the Sycamore Formation reveal a number of different magnetic fabrics caused by the synergy between diagenetic, tectonic, and hydrodynamic processes.

Vertical to sub-vertical K1 tensors in the uppermost and lowermost sites (sites 7 and 9) of the Sycamore Formation suggest the presence of an inverse AMS fabric, especially when displayed in stratigraphic or tilt-corrected coordinates (Figure 28). Inverse fabrics result from an inverse relationship between magnetic axes and crystallographic axes where K1 is parallel to Z and K3 is parallel to X (e.g., Rochette, 1988; Ihmlé et. al., 1989; Ferré, 2002). Single-domain magnetite or iron-bearing carbonates such as siderite, ankerite, and Fe-bearing dolomite are common inverted fabric carriers (Rochette, 1988; Heij et. al., 2018). SEM analysis shows evidence of abundant ferroan dolomite in the Lower Sycamore Section, specifically in site 7 (Figures 14C and 15) indicating alteration by iron-rich dolomitizing fluids. The ferroan dolomite occurs as grains both in the matrix and vertical veins as well as authigenic rims on dolomite grains. The occurrence of Fe-dolomite suggests that it is the explanation for the inverted AMS fabric in the Sycamore Formation. Intermediate AMS fabrics are also likely to occur if there is a combination of a normal and inverse magnetic fabric (Ferré, 2002).

The strong bedding-parallel lineation observed in site 3 (Figure 29) with an approximately N-S alignment of K1 tensors indicates that the grains of longer axes could be parallel to current

flow directions (e.g., Hrouda, 1982). The slightly inclined K1 (0.6°) in site 3 (stratigraphic coordinates) suggests flow in the up-current direction, which in this case would represent a north to south flow direction (e.g., Schieber and Ellwood, 1988). The inclination is only very slight, and the results from site 3 could still indicate either N-S or S-N currents. The outcrop lithofacies located in site 3 have been reported to contain current lineations, planar laminations, and other sedimentary structures associated with Bouma sequences (Ta and Tb) (e.g., Milad, 2019). The relationship between grain alignment and flow direction is dependent on a series of moderate or high hydrodynamic regimes (Heij et. al., 2015).

Certain sites could be interpreted as containing partial diagenetic fabrics where authigenic alteration of mineral phases resulted in new preferred orientation by changing the original AMS fabric. The growth of new mineral phases can distort the original fabric particularly in cases where the mineral volume exceeds the only space available for mineral growth (Heij et. al., 2015). As previously mentioned, inverted fabrics caused by ferroan dolomite are found in specimens of the Sycamore Formation. Moreover, the occurrence of mineralized fractures with possible stylolites (Figure 19B) may suggest fluid-flow interactions which could lead to diagenetic alteration of magnetic fabrics and the development of non-planar fabrics. This hypothesis could serve as an explanation for the AMS fabrics in sites 2 and 6 (Figure 31).

Petrographic analysis from the Middle Sycamore Section also reveals evidence of slip along the edge of vertical veins due to movement caused by deformation. This observation implies that deformation may also have contributed to the AMS fabrics of the Sycamore Formation. I note, however, that there are no sites where K1 is perpendicular to the shortening direction (ESE-WNW) although there are instances (Site 8; Figure 30) where a few specimens display WNW directions. Though deformation is probably not a major contributor to the AMS fabrics (e.g., Parés, 2015,

Dudzisz et. al., 2016), most fabrics in the Sycamore Formation are interpreted as representing composite fabrics with possible diagenetic (alteration by Fe-rich dolomitizing fluids), tectonic, and hydrodynamic influence (e.g., third group of AMS fabrics- sites 2, 6, and 8; Figures 30 and 31).

The majority of the AMS results from the Sycamore Formation are very complex and probably represent composite fabrics (Figures 30 and 31). It is worthwhile to note that composite fabrics between diagenetic, primary hydrodynamic, and tectonic processes are possible in the Sycamore Formation, especially in sites with AMS ellipsoids displaying principal axis striking in multiple directions (Site 8; Figure 30). In these instances, data interpretation is very difficult accounting for the lack of active research on magnetic fabrics of siltstones as well as the complexities of factors controlling the development of AMS fabrics in siltstones.

CONCLUSIONS

The Sycamore Formation displays significant diagenetic alteration through multiple dissolution, fracturing, mineralization, and brecciation events. A plethora of early to middle diagenetic events occur within the matrix and allochems at relatively low pressures and temperatures. During deeper burial at relatively high temperatures, other diagenetic events occurred especially those within mineralized fractures.

Sycamore rocks are characterized by precipitation of two main types of cement- an intergranular calcite cement and a blocky pervasive calcite cement. The pervasive calcite cement is syn-sedimentary based on the “floating texture” of the grains and early dissolution of skeletal allochems. The intergranular calcite cement generally occurs in mudrocks and calcitic siltstone microfacies while the pervasive calcite cement dominates the calcite cemented siltstones. The intergranular calcite cement precipitated as a result of dissolution of allochems and unstable feldspar grains, and during clay alteration in the course of early to middle diageneses.

Pore development in Sycamore rocks was a relatively continuous process defined by early evolution of intergranular porosity associated with clay structure and other framework grains. Dissolution porosity is burial in origin as a consequence of feldspar dissolution which is common in the calcitic siltstone facies. Therefore, the calcitic siltstone microfacies is locally more porous than the calcite cemented siltstones since the pervasive calcite cement in the latter occludes the porosity.

Anisotropy of magnetic susceptibility fabrics are composite, representing a combination of diagenetic, tectonic, and depositional fabrics. An inverted magnetic fabric is attributed to the occurrence of ferroan dolomite. The dolomite and inverse fabric relate to alteration by iron-rich dolomitizing fluids.

The Sycamore Formation was primarily a system dominated by internal fluids. Diagenetic events such as illitization, dewatering of shales, maturation of organic matter, and dissolution of microorganisms and allochems are internally responsible for most of the diagenetic reactions within the system. During burial, the Sycamore Formation might have evolved into an open fluid-dominated system allowing alteration (e.g., dissolution of feldspars) by external fluids. These fluids include iron-rich dolomitizing fluids and/or organic acidic-rich fluids deriving from hydrocarbon maturation in the underlying Woodford Shale.

Although some mineral phases (e.g., barite and apatite) that have been tied to hydrothermal alteration were observed in Sycamore microfacies, there is no strong evidence for hydrothermal alteration in the Sycamore Formation. The magnetizations in the unit are CRMs residing in magnetite, but the timing of remagnetization cannot be determined because a fold test could not be performed.

REFERENCES

Al-Ramadan, K., Morad, S., Proust, J.N., and Al-Aasm, I.S., (2005). Distribution of diagenetic alterations in siliciclastic shoreface deposits within a sequence stratigraphic framework: Evidence from the Upper Jurassic, Boulonnais, NW France. *Journal of Sedimentary Research*, Vol. 75, p. 943–959, doi:10.2110/jsr.2005.072.

Allen, R. W. (2000). Complex Structural Features of the Ardmore Basin: Oklahoma City. *Geological Society in the Shale Shaker*, v. 51.

Bennison, A.P. (1956). Springer and Related Rocks of Oklahoma. *Tulsa Geological Society Digest*, Vol. 24, p. 112.

Berner, R.A., Leeuw, J. W., Spiro, B., Murchison, D.G., and Eglinton, G. (1985). Sulphate reduction, organic matter decomposition and pyrite formation. *Philosophical Transactions of the Royal Society of London. Series A, Mathematical and Physical Sciences*, Vol. 315, 25-38, doi: 10.1098/rsta.1985.0027.

Bjørlykke, K., Mo, A., and Palm, E. (1988). Modelling of thermal convection in sedimentary basins and its relevance to diagenetic reactions. *Marine and Petroleum Geology*, 5(4), 338-351.

Bjorlykke, K., and Egeberg, P. K. (1993). Quartz cementation in sedimentary basins. AAPG bulletin, 77(9), 1538-1548.

Bjorlykke, K., and Jahren, J. (2012). Open or closed geochemical systems during diagenesis in sedimentary basins: Constraints on mass transfer during diagenesis and the prediction of porosity in sandstone and carbonate reservoirs: *American Association of Petroleum Geologists Bulletin*, 2193-2214.

Blakey, Ronald C., 2013, Using Paleogeographic Maps to Portray Phanerozoic Geologic and Paleotectonic History of Western North America: *Search and Discovery*, no. 30267.

Blatt, H. (1982). Sedimentary Petrology. W. H. Freeman and Co., San Francisco.

Blomme, K., Fowler, S. J., Bachaud, P., Nader, F. H., Michel, A., and Swennen, R. (2017). Ferroan Dolomitization by Seawater Interaction with Mafic Igneous Dikes and Carbonate Host Rock at the Latemar Platform, Dolomites, Italy: Numerical Modeling of Spatial, Temporal, and Temperature Data. *Geofluids*, *2017*, 6590672. https://doi.org/10.1155/2017/6590672.

Boles, J., and Franks, S. (1979). Clay Diagenesis in Wilcox Sandstones of Southwest Texas. *Implications of Smectite Diagenesis on Sandstone Cementation*, *49*.

Bouzari, F. B., Hart, C. J. R., Bissig, T., and Barker, S. (2016). Hydrothermal alteration revealed by apatite luminescence and chemistry: A potential indicator mineral for exploring covered porphyry copper deposits. *Economic Geology*, 111, 1397–1410.

Brenner, R. L., Ludvigson, G., Scal, R., and Dogan, A. (2010). Diagenetic modeling of siliciclastic systems: Status report. *Kansas Geological Survey Bulletin*, *233*, 123–137.

Butler, R. (1992). Paleomagnetism: Magnetic domains to geologic terranes. Boston: Blackwell Scientific Publications.

Cardott, B. J. (2012). Thermal maturity of Woodford Shale gas and oil plays, Oklahoma, USA. *International Journal of Coal Geology*, v. 103, p. 109–119, doi:10.1016/j.coal.2012.06.004.

Cardott, B.J., and Chaplin, J.R., (1993). Guidebook for selected stops in the western Arbuckle Mountains, southern Oklahoma: *OGS Special Publication* 93-3, 55.

Cardott, B.J., Metcalf, W.J., and Ahern, J.L. (1990). Thermal maturation by vitrinite reflectance of Woodford Shale near Washita Valley fault, Arbuckle Mountains, Oklahoma. Applications of thermal maturity studies to energy exploration: SEPM Rocky Mountain Section, 139-146.

Caylor, S. (2019). Characterization of the Sycamore Formation, Velma Field, Ardmore Basin, Oklahoma. The University of Oklahoma, Masters Thesis.

Chadima, M., and Jelinèk, V. (2009). Anisoft 4.2: anisotropy data browser for windows. Agico. Inc, Brno. https://www.agico.com/text/software/anisoft/anisoft.php.

Champlin, S.C. (1959). A Stratigraphic Study of the Sycamore and Related Formations in the Eastern Arbuckle Mountains. The University of Oklahoma, Masters Thesis.

Coffey, W.S. (2000). The Diagenetic History and Depositional System of the Sycamore Formation (Mississippian), Carter-Knox Field, Grady and Stephens Counties, Oklahoma. Oklahoma State University, Dissertation.

Cole, T. (1988). A surface to Subsurface Study of the Sycamore Limestone (Mississippian) along the North Flank of the Arbuckle Anticline, University of Oklahoma. The University of Oklahoma, Masters Thesis.

Cooper, C.L. (1926). The Sycamore Limestone, Oklahoma Geological Survey, Circular No.9.

Culp, C.K. (1961). Stratigraphic Relations of the Sycamore Limestone (Mississippian) in Southern Oklahoma, *Shale Shaker*, Vol. 11, No. 10, 7-18.

Curtis, D. M., and Champlin, S. C. (1959). Depositional Environments of Mississippian Limestones of Oklahoma. *Tulsa Geological Society Digest*, v. 27, 90–103.

Dehcheshmehi, S., Gregg, J. M., Grammer, M., Puckette, J., Shelton, K., and White, J. (2016). Regional Diagenesis of Mississippian Strata of the Southern Mid-Continent, USA. ProQuest Dissertations and Theses.

Domeier, M. (2015). A plate tectonic scenario for the Iapetus and Rheic oceans. *Gondwana Research, 36*(C), 275-295.

Donovan, R. N. (2001). Field Study of the Sycamore Formation on Interstate Highway 35 in the Arbuckle Mountains, Oklahoma, in Johnson, K.S. (ed.), Silurian, Devonian, and Mississippian geology and petroleum in the southern Midcontinent, 1999 symposium: Oklahoma Geological Survey Circular 105, 139-149.

Duarte Coronado, D. (2018). Rock Characterization and Stratigraphy of the Mississippian Strata, Meramec/Sycamore. Merge Play, Central Oklahoma. The University of Oklahoma, Masters Thesis.

Dudzisz, K., Szaniawski, R., Michalski, K., and Manby, G. (2016). Applying the anisotropy of magnetic susceptibility technique to the study of the tectonic evolution of the West Spitsbergen Fold-and-Thrust Belt. *Polar Research*, 35(1), 31683-12.

Ehrenberg, S. N., and Jakobsen, K. G. (2001). Plagioclase dissolution related to biodegradation of oil in Brent Group sandstones (Middle Jurassic) of Gullfaks Field, northern North Sea. *Sedimentology*, 48(4), 703-721.

Elmore, R. D., Muxworthy, A. R., Aldana, M. and Mena, M. (2012). Remagnetization and Chemical Alteration of Sedimentary Rocks, *Geological Society,* London, Special Publications 371, doi: 10.1144/SP371.15.

Elmore, R. (2001). A review of palaeomagnetic data on the timing and origin of multiple fluid-flow events in the Arbuckle Mountains, southern Oklahoma. *Petroleum Geoscience*, 7(3), 223-229.

Elmore, R. D., and Crawford, L. (1990). Remanence in authigenic magnetite: Testing the hydrocarbon-magnetite hypothesis. *Journal of Geophysical Research: Solid Earth*, 95(B4), 4539-4549.

Elmore, R. D. (2001). A Review of Paleomagnetic Data on the Timing and Origin of multiple Fluid-Flow Events in the Arbuckle Mountains, Southern Oklahoma. *Petroleum Geoscience*, 7, 223-229.

Elmore, R.D., Campbell, T., Banerjee, S., Bixler, W.G. (1998). Paleomagnetic dating of ancient fluid-flow events in the Arbuckle Mountains, southern Oklahoma. In: PARNELL, J. (ed.) 1998. Dating and Duration of Fluid Flow and Fluid-Rock Interaction. *Geological Society*.

Elmore, Richard D., Justin, H., Sarah, F., and Simon, A. (2017). Integrated paleomagnetic and diagenetic study of the Mississippian Limestone, North Central Oklahoma: *AAPG Memoir 116*, doi10.1306/13632156M11667.

Er, C., Li, Y., Zhao, J., Wang, R., Bai, Z., and Han, Q. (2016). Pore formation and occurrence in the organic-rich shales of the Triassic Chang-7 Member, Yanchang Formation, Ordos Basin, China. *Journal of Natural Gas Geoscience*, *1*. https://doi.org/10.1016/j.jnggs.2016.11.013.

Fay, R. O. (1989). Geology of the Arbuckle Mountains along Interstate - 35, Carter and Murray Counties, Oklahoma.

Ferré, E. C. (2002). Theoretical models of intermediate and inverse AMS fabrics. *Geophysical Research Letters*, 29(7), 1127-31-4.

Fisher, R. (1953). Dispersion on a Sphere. *Proceedings of the Royal Society of London. Series A, Mathematical and Physical Sciences* (1934-1990), 217(1130), 295-305.

Folk, Robert L. (2005). Nannobacteria and the formation of framboidal pyrite: Textural evidence. *Journal of Earth System Science*, 114(3), 369-374.

Franklin, K.E. (2002). The depositional History of the Sycamore Limestone, Oklahoma State University, Thesis.

Galvis Portilla, H. (2017). Detailed Lithostratigraphic Characterization and Sequence Stratigraphy of a Complete Woodford Shale Outcrop Section in Southern Oklahoma. The University of Oklahoma, Masters Thesis.

García-Lasanta, C., Oliva-Urcia, B., Román-Berdiel, T., Casas, A. M., and Pérez-Lorente, F. (2013). Development of magnetic fabric in sedimentary rocks: Insights from early compactional structures. *Geophysical Journal International, 194*(1), 182-199.

Granath, J. W. (1989). Structural evolution of the Ardmore Basin, Oklahoma: Progressive deformation in the foreland of the Ouachita Collision. *Tectonics*, *8*(5), 1015–1036.

Ham, W., Stitt, James H., Derby, James R., Fay, Robert O., and Graffham, Allen A. (1969). Geology of the Arbuckle Mountains. *Oklahoma Geological Survey*.

Ham, W.E., and McKinley, M.E. (1954). Geological Map and Sections, Arbuckle Mountains, OK. revised by Johnson, K.S., 1990. Oklahoma Geo-logical Survey, Circular 91.

Hanor, J. S. (2000). Barite-celestine geochemistry and environments of formation. *Reviews in Mineralogy and Geochemistry*, v. 40, no. 1, 193–275.

Hardwick, J. (2018). Reservoir Quality Evaluation of the Meramec and Upper Osage Units in the Anadarko Basin. The University of Oklahoma, Masters Thesis.

Heij, G., Elmore, D., Roberts, J., Steullet, A. K., Dulin, S., and Friedman, S. (2015). Anisotropy of Magnetic Susceptibility: A Petrofabric Tool to Measure the Fabric of Shales. Unconventional Resources Technology Conference. doi:10.15530/URTEC-2015-2170863.

Heij, G. (2018). Magnetic Fabrics and Paleomagnetism of North American Mudrocks: Relics of Complex Burial Histories. Doctoral dissertation, University of Oklahoma, Norman, Oklahoma.

Heij, G., Elmore, R., Dulin, S., Sondergeld, C., Roger, S., and Ferre, E. (2018). Magnetic Fabrics and Paleomagnetism of North American Mudrocks: Relics of Complex Burial Histories.

Hrouda, F. (1982). Magnetic anisotropy of rocks and its application in geology and geophysics. *Geophysical Surveys*, 5(1), 37-82.

Ihmlé, P.F., Hirt, A.M., Lowrie, W. and Dietrich, D. (1989). Inverse magnetic fabric in deformed limestones of the Morcles Nappe, Switzerland. *Geophysical Research Letters*, 16(12), 1383-1386.

Jackson, J., Calvin, J., and Drake, B. (2018). Stimulation Design and Treatment in the Sycamore Formation of the South-Central Oklahoma Oil Province Area of the Anadarko Basin. *SPE-189869-MS*, 17.

Jelinèk, V. (1981). Characterization of the magnetic fabric of rocks. *Tectonophysics*, 79(3-4), pp. T63-T67.

Kirschvink, J.L. (1980). The least-squares line and plane and the analysis of paleomagnetic data.

Krajewski, K., and WOŹNY, E. (2009). Origin of dolomite–ankerite cement in the Bravaisberget Formation (Middle Triassic) in Spitsbergen, Svalbard. *Polish Polar Research - POL POLAR RES*, *30*, 231–248. https://doi.org/10.4202/ppres.2009.11.

Land, L.S., Mack, L.E., Milliken, K.L. and Lynch, F.L. (1997). Burial diagenesis of argillaceous sediment, south Texas Gulf of Mexico sedimentary basin: A reexamination: *Geological Society of America Bulletin*, 109, 2–15, London, Special Publications, 144, 9-25.

Lazar, O.R., Bohacs, K.M., Macquaker, J.H.S., Schieber, J., Demko, T.M. (2015). Integrated approach for the nomenclature and description of the spectrum of fine-grained sedimentary rocks. *J. Sediment. Res.* 85, 230–246.

Machel, H. G., and Lonnee, J. (2002). Hydrothermal dolomite: A product of poor definition and imagination. *Sedimentary Geology*, 152, 163–171, doi: 10.1016/S0037-0738(02)00259-2.

McCabe, C., and Elmore, R. D., 1989. The occurrence and origin of Late Paleozoic remagnetization in the sedimentary rocks of North America. *Rev. Geophys*., 27 (4), 471– 494.

Miceli Romero, A. and Philp, R.P. (2012). Organic geochemistry of the Woodford Shale, southeastern Oklahoma; how variable can shales be? AAPG Bulletin, 96, 493–517, doi: 10.1306/08101110194

Milad, B. (2019). Integrated Reservoir Characterization and Geological Upscaling for Reservoir Flow Simulations of the Sycamore/Meramec and Hunton Plays in Oklahoma.

Miller, J., and Cullen, A. (2018). My Favorite Outcrop: Sycamore Formation I-35 South, Arbuckle Mountains, OK. *The Shale Shaker,* vol.69, no.82, p. 87-99.

Miller, J. (2018). Regional Stratigraphy and Organic Richness of the Mississippian Meramec and Associated Strata, Anadarko Basin, Central Oklahoma. The University of Oklahoma.

Milliken, K., and Olson, T. (2017). Silica diagenesis, porosity evolution, and mechanical behavior in siliceous mudstones, Mowry Shale (Cretaceous), Rocky Mountains, USA. *Journal of Sedimentary Research*, v. 87, p. 366–387, doi: 10.2110/jsr.2017.24.

Milliken, L., and Olson, T. (2017). Silica diagenesis, porosity evolution, and mechanical behavior in siliceous mudstones, Mowry Shale (Cretaceous), Rocky Mountains, U.S.A. *Journal of Sedimentary Research*, 87(4), 366-387.

Molenaar, N. (1990). Calcite cementation in shallow marine Eocene sandstones and constraints of early diagenesis. *Journal of the Geological Society*, 147(5), 759-768.

Moore, C. (2001). Carbonate reservoirs: Porosity evolution and diagenesis in a sequence stratigraphic framework. *Developments in sedimentology*, 55.

Morad, S., Al-Aasm, I., Ramseyer, K., Marfil, R., and Aldahan, A. (1990). Diagenesis of carbonate cements in Permo-Triassic sandstones from the Iberian Range, Spain: evidence from chemical composition and stable isotopes. *Sedimentary Geology*, v. 67, no. 3–4, 281–295, doi:10.1016/0037-0738(90)90039-V.

Nesse, W. D. (2017). Introduction to mineralogy. New York: Oxford University Press, 395.

Nojek, A. and Li, Y. (2017). How central Oklahoma's SCOOP/STACK shale plays are stacking up against the competition: McKinsey Energy Insights.

Northcutt, R.A. and Campbell, J.A (1998). Geologic Provinces of Oklahoma: Basement Tectonics, 12, 29-37.

Northcutt, R. A., Johnson, K.S., and Hinshaw, G. C. (2001) Geology and petroleum reservoirs in Silurian, Devonian, and Mississippian rocks in Oklahoma. In Silurian, Devonian, and Mississippian geology and petroleum in the southern mid-continent: 1999 Symposium Oklahoma Geological Survey Circular, 105, 1-29.

Palladino, D.L. (1985). Tectonism and Sedimentation in the Arbuckle Mountain Region, Southern Oklahoma Aulacogen, Baylor University, Waco, Texas.

Parés, J. M. (2015). Sixty years of anisotropy of magnetic susceptibility in deformed sedimentary rocks. *Frontiers in Earth Science (Lausanne*), vol.3.

Perry, W. J. (1989). Tectonic Evolution of the Anadarko Basin Region, Oklahoma: Denver, United State Government Printing Office.

Pevear, D. R. (1999). Illite and hydrocarbon exploration: Proceedings of the National Academy of Sciences, 96, 3440–3446, doi:10.1073/pnas.96.7.3440.

Pittman, E., Larese, R., and Heald, M. (1992). Clay coats: Occurrence and relevance to preservation of porosity in sandstones (Vol. 47, pp. 241–255). https://doi.org/10.2110/pec.92.47.0241.

Prestridge, J.D. (1957). A subsurface Stratigraphic Study of the Sycamore Formation in the Ardmore Basin. The University of Oklahoma, Masters Thesis.

Price, J., Pollack, A.C., Lamb, A. P., Peryam, T.C, and Anderson, J. R. (2020). Depositional interpretation and sequence stratigraphic control on reservoir quality and distribution in the Meramecian Sooner Trend Anadarko Basin, Canadian, and Kingfisher Counties (STACK) play, Anadarko Basin, Oklahoma, United States. *AAPG Bulletin, 104*(2), 357-386.

Prothero, D., & Schwab, F. L. (2013). Sedimentary geology: An introduction to sedimentary rocks and stratigraphy (Third ed.).

Rahman, M. J. J., and Worden, R.H. (2016). Diagenesis and its impact on the reservoir quality of Miocene sandstones (Surma Group) from the Bengal Basin, Bangladesh. *Marine and Petroleum Geology*, v. 77, p. 898–915, doi:10.1016/j.marpetgeo.2016.07.027.

Ries, J. B. (2010). Review: Geological and experimental evidence for secular variation in seawater Mg/Ca (calcite-aragonite seas) and its effects on marine biological calcification. *Biogeosciences,* 7(9), 2795-2849.

Roberts, J., Heij, G., and Elmore, R. (2019). Paleomagnetic dating of hydrothermal alteration in the Woodford Shale, Oklahoma, USA. *Geological Magazine*, 1-10.

Rochette P., Jackson M., and Aubourg C. (1992). Rock magnetism and the interpretation of anisotropy of magnetic susceptibility. *Reviews of Geophysics*, 30, 209-226.

Rochette, P. (1987). Magnetic susceptibility of the rock matrix related to magnetic fabric studies. *Journal of Structural Geology*, 9(8), 1015-1020.

Rochette, P. (1988). Inverse magnetic fabric in carbonate-bearing rocks. *Earth and Planetary Science Letters*, 90(2), 229-237.

Sassen, R., Moore, C.H., and Meendsen, F.C. (1987). Distribution of hydrocarbon source potential in the Jurassic Smackover Formation. *Organic Geochemistry*, v.11, 379-383.

Schieber, J. (2011). Iron Sulfide Formation. *Encyclopedia of Geobiology*, 486-502.

Schieber, J., and Ellwood, B. B. (1993). Determination of basinwide paleocurrent patterns in a shale succession from anisotropy of magnetic susceptibility (AMS): a case study of the mid-Proterozoic Newland formation, Montana. *Journal of Sedimentary Research*, 63(5).

Schieber, J., Krinsley, D., and Riciputi, L. (2000). Diagenetic origin of quartz silt in mudstones and implications for silica cycling. *Nature*, 406, 981-985, doi: 10.1038/35023143.

Schieber, J., Ellwood, B. (1988). The Coincidence of Macroscopic Paleocurrent Indicators and Magnetic Lineation in Shales from the Precambrian Belt Basin. *SEPM Journal of Sedimentary Research*, *Vol. 58*. https://doi.org/10.1306/212F8E7C-2B24-11D7-8648000102C1865D.

Schwartzapfel, J.A. (1990). Biostratigraphic Investigations of Late Paleozoic (Upper Devonian to Mississippian) Radiolaria within the Arbuckle Mountains and Ardmore Basin of South-Central Oklahoma, University of Texas at Dallas, Dissertation, pp. 11-23, 333-336.

Sivalingam, S. (1990). Clay diagenesis of the source rocks from the Permian Basin: Doctoral dissertation, Texas Tech University, 263 p.

Sun, N., Zhong, J., Hao, B., Ge, Y., and Swennen, R. (2019). Sedimentological and diagenetic control on the reservoir quality of deep-lacustrine sedimentary gravity flow sand reservoirs of the Upper Triassic Yanchang Formation in Southern Ordos Basin, China. *Marine and Petroleum Geology*, v. 112, no. September 2019, p. 104050.

Taff, J.A. (1903). Geologic Atlas of the United States, Tishomingo Folio, Indian Territory, No. 98, p.5.

Tarling, D.H. & Hrouda, F. (1993). The Magnetic Anisotropy of Rocks, Chapman & Hall, London, 215pp.

Terrell, C. (2019). Regional Stratigraphy and Diagenetic Characterization of the Mississippian Meramec, Osage, and Sycamore Formations, Anadarko Basin, Central Oklahoma. The University of Oklahoma, Masters Thesis.

Thyberg, B., Jahren, J., Turid, W., Knut, B., Ingle, F., and Oyvind, M. (2010). Quartz Cementation in Late Cretaceous Mudstones, Northern North Sea: Changes in Rock Properties Due to Dissolution of Smectite and Precipitation of Micro-Quartz Crystals. *Marine and Petroleum Geology*, v. 27, no. 8, p. 1752–1764, doi 10.1016/j.marpetgeo.2009.07.005.

Torsvik, T.H., Van der Voo, R., Preeden, U., Niocaill, C.M., Steinberger, B., Doubrovine, P.V., Douwe J.J.., Domeier, M., Gaina, C., Tohver, E., Meert, J.G., McCausland, J.A., Robin, L., Cocks, M. (2012). Phanerozoic Polar Wander, Palaeogeography and Dynamics. *Earth-Science Reviews*, 114, 325-68, doi: 10.1016/j.earscirev.2012.06.007.

Ulmer-Scholle, D. S., Scholle, P. A., Schieber, J., and Raine, R. J. (2015). A Color Guide to the Petrography of Sandstones, Siltstones, Shales and Associated Rocks. Tulsa, OK. American Association of Petroleum Geologists.

Walderhaug, O. (2000). Modeling quartz cementation and porosity in Middle Jurassic Brent Group sandstones of the Kvitebjørn field, northern North Sea. AAPG bulletin, 84(9), 1325-1339.

Wang, P., Jiang, Z., Ji, W., Zhang, C., Yuan, Y., Chen, L., and Yin, L., (2016). Heterogeneity of intergranular, intraparticle and organic pores in Longmaxi shale in Sichuan Basin, South China: Evidence from SEM digital images and fractal and multifractal geometries. *Marine and Petroleum Geology*, 72, 122-138.

White, D. E. (1957). Thermal waters of volcanic origin. *Geological Society of America Bulletin*, 68, 1637–1658, doi: 10.1130/0016-7606(1957)68[1637:TWOVO]2.0.CO;2.

Woods, S., Elmore, R. D., and Engel, M. (2002). Paleomagnetic dating of the smectite-to-illite conversion: testing the hypothesis in Jurassic sedimentary rocks, Skye, Scotland. *Journal of Geophysical Research*, 107, 2091, http://dx.doi.org/10.1029/2000JB000053.

Worden, R. H., and Barclay, S.A. (2000). Internally sourced quartz cement due to externally derived CO2 in sub-arkosic sandstones, North Sea. *Journal of Geochemical Exploration*. doi:10.1016/S0375-6742(00)00104-7.

Xiong, D., Azmy, K., and Blamey, N. J. F. (2016). Diagenesis and origin of calcite cement in the Flemish Pass Basin sandstone reservoir (Upper Jurassic): Implications for porosity development. *Marine and Petroleum Geology*, v. 70, p. 93–118, doi:10.1016/j.marpetgeo.2015.11.013.

Yuan, G., Cao Y., Gluyas, J., Li X., Xi K., Wang Y., Oxtoby, N. H. (2015). Feldspar dissolution, authigenic clays, and quartz cements in open and closed sandstone geochemical systems during diagenesis; typical examples from two sags in Bohai Bay Basin, east China. AAPG Bulletin, 99(11), 2121-2154.

Zhang, R., Hu, S., Zhang, X., & Yu, W. (2007). Dissolution Kinetics of Dolomite in Water at Elevated Temperatures. *Aquatic Geochemistry*, *13*, 309–338. https://doi.org/10.1007/s10498-007-9022-z

Zhang, S., Liu, H., Wang, M., Liu, X., Liu, H., Bao, Y., and Fang, Z. (2019). Shale pore characteristics of Shahejie Formation: Implication for pore evolution of shale oil reservoirs in Dongying sag, north China. *Petroleum Research, 4*(2), 113-124.

Zijderveld, J.D.A. (1967). A.C. demagnetization of rocks: Analysis of results. In: Collinson, D. E., Creer, K. M. & Runcorn, S. K. (eds) 1967. Methods in Paleomagnetism, 254- 286.